

Complementary Signatures for Strongly Interacting Dark Matter

A Thesis

submitted to

Indian Institute of Science Education and Research Pune

in partial fulfillment of the requirements for the

BS-MS Dual Degree Programme

by

Saptarshi Pal



Indian Institute of Science Education and Research Pune

Dr. Homi Bhabha Road,
Pashan, Pune 411008, INDIA.

May, 2023

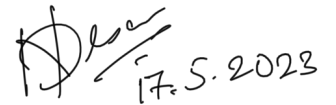
Supervisor: Dr. Nishita Desai

© Saptarshi Pal 2023

All rights reserved

Certificate

This is to certify that this dissertation entitled Complementary Signatures for Strongly Interacting Dark Matter towards the partial fulfilment of the BS-MS dual degree programme at the Indian Institute of Science Education and Research, Pune represents study/work carried out by Saptarshi Palat Indian Institute of Science Education and Research under the supervision of Dr. Nishita Desai, Ramanujan Fellow, Department of Theoretical Physics, TIFR Mumbai, during the academic year 2018-2023.



Dr. Nishita Desai

Committee:

Dr. Nishita Desai

Dr. Seema Sharma

This thesis is dedicated to my grandparents

Declaration

I hereby declare that the matter embodied in the report entitled Complementary Signatures for Strongly Interacting Dark Matter are the results of the work carried out by me at the Department of Theoretical Physics, TIFR Mumbai, Indian Institute of Science Education and Research, Pune, under the supervision of Dr. Nishita Desai and the same has not been submitted elsewhere for any other degree.

A handwritten signature in black ink that reads "Saptarshi Pal". The signature is written in a cursive style with a long horizontal stroke at the end of the word "Pal".

Saptarshi Pal

Acknowledgments

I start by acknowledging my supervisor Dr. Nishita Desai, who has been a mentor to me far beyond the thesis. We have been working together from the times of the infamous COVID19 pandemic, and she helped me, and picked me up, at a time when I was at a low juncture of my academic journey. I shall forever be grateful to her for her immense patience with me despite my shortcomings. Her guidance throughout the course of the 2 years that we worked together, specifically during the fifth year, for both, my academic and non-academic concerns, has left me deeply indebted to her. I couldn't have asked for someone better, as my guide. I thank my TAC member, Dr. Seema Sharma who presented me with this wonderful opportunity to work with Dr. Desai, and has always been present to help me with anything in IISER Pune. I also want to acknowledge Dr. Surjeet Singh for accepting me to work in his lab, and mentoring me as one of his beloved students, despite the short duration of my project with him. He's always motivated and comforted me and I am deeply grateful.

I want to acknowledge every person who's been a constant throughout the last 5 years, starting with the usual suspects, my parents, Tania and Sushovan (without whom, realising this dream wouldn't have been possible), my brother and sister, Rajarshi and Titas (my main source of motivation), grandparents, maternal uncles and aunt (who seem more interested in my work than me myself), my dearest friends back home, and everyone in my extended family. I would particularly like to thank Rishabh and the Sen family, Torsha, Chandrima, Amitava and Aranya, for very much being a part of this BS-MS journey (and lighting up my life in more ways than they will ever know).

Finally, I want to thank my entire support system in IISER Pune, who made this journey memorable. I want to specially acknowledge my room-mate and close friend, Rajat who helped me with all my doubts in physics throughout the duration along with Aviral; the three of us had really illuminating discussions on physics. I also want to acknowledge my

friend Saksham for helping me with various technical doubts related to computations. I would like to thank all of my other friends in IISER, with special mentions of Varun, Rupal, Prem and Aishwarya. I thank IISER Pune, for accepting me and enabling this unique experience, and TIFR Mumbai for hosting me during a part of my thesis.

Abstract

The field of Beyond the Standard Model phenomenology is rich with possibilities and presents us with a variety of potentially new and interesting answers which would eventually help us understand the small-scale, as well as the large-scale structure of our universe better. Hence, an appropriate extension of our current understanding of the Standard Model with Dark Matter, providing results and predictions which can be verified to high accuracy is very desirable. A possible solution to this is a hidden and confined DM sector with strong self-interaction of the particles, similar to mesons in QCD. Building such a model and probing its existence is explored in this project. In this model we find that multiple annihilation mechanisms can work to give us the correct relic density of dark matter. We show that this model cannot give us a signal through Direct Detection experiments. We also show how Indirect Detection signatures can be used to probe the phase space of the model.

Contents

Abstract	xi
1 Preliminaries	5
1.1 Introduction	5
1.2 Astronomical Observations of Dark Matter	7
1.3 Overview of DM detection techniques	7
1.4 Scattering and Decays	8
2 Calculating Dark Matter Density	13
2.1 Thermal Relic density and Freeze-out	13
2.2 Simplified dark matter model with spin-0 mediator	18
2.3 Simplified dark matter model with spin 1 mediator	21
2.4 The Freeze-in mechanism and the FIMPs	25
3 Strongly Interacting Dark Matter	33
3.1 A model of Dark Pions	33
3.2 Adding a $U(1)'$ charged vector boson Z'	43
4 Complementary Signatures of SIDM	51

4.1 Direct Detection of Dark Matter	51
4.2 Indirect Detection of Dark Matter	52
5 Conclusion	57
Appendices	59
A	61
A.1 Calculation techniques for Scattering Amplitudes and Cross-section matrices	61
A.2 Calculation of σ for the release of dark photons from dark fermions in terms of s	76
A.3 Useful Dirac algebra properties and proofs	77

List of Figures

1.1 Schematic of the various detection possibilities for DM [1]	8
2.1 An illustration of the DM Relic density before and after thermal Freeze-out (z_f) of WIMP	14
2.2 Feynman diagram for the simplified DM model with spin-0 mediator	19
2.3 Exploring the value of the RD over the parameter space for the spin-0 mediator model.	20
2.4 Feynman diagram for the simplified DM model with spin-1 mediator	21
2.5 Exploring the value of the RD over the parameter space for the spin-1 mediator model: changes in mass parameters.	23
2.6 Exploring the value of the RD over the parameter space for the spin-1 mediator model: changes in coupling parameters.	24
2.7 Feynman diagrams for processes contributing to the Freeze-in model.	28
2.8 Simulation of DM density for the Freeze-in scenario.	32
3.1 The main annihilation channels for DM to SM energy transfer via unstable dark pion to SM fermions	35
3.2 DM to SM decay via an additional Z' vector mediator which can decay into SM fermions	35
3.3 Freeze-out temperatures for different DM mass candidates of the simplified model.	36

3.4	Plots for the coupling coefficients corresponding to the vertex between the π_d and π_c in order to get the observed RD for the simplified model.	37
3.5	Freeze-out temperature for different DM mass candidates of the model.	40
3.6	A plot showing the coupling (which has been written in terms of the pion decay factor f) required to give the observed value of RD for different masses of DM.	41
3.7	A plot showing the value of f required to give the observed value of RD for different values of DM masses.	41
3.8	A plot showing the value of f required to get the correct RD for values of m_{DM} ranging from 1-100 GeV and each with four different cases of percentage difference between masses of π_c and π_d .	42
3.9	A plot showing the point of intersection between the $\Omega h^2 = 0.112$ line and the curve which shows how the RD changes with the mass of the DM.	44
3.10	Change in RD with DM mass for the Z' Channel.	45
3.11	Change in RD with DM mass for the Z' channel while also varying the coupling, g'_{DM} .	46
3.12	RD values while scanning $m_{Z'}$ from 50 GeV - 400 GeV and m_{DM} scanned from 25 GeV - 250 GeV.	47
3.13	Contour plot for the RD values while scanning $m_{Z'}$ from 50 GeV - 400 GeV and m_{DM} scanned from 25 GeV - 250 GeV along with percentage contribution from the strong channel.	48
3.14	The contour plot for mapping the RD whilst varying the parameters f and $m_{Z'}$ across the larger ranges, $f = 50 - 1000$ and $m_{Z'} = 100 - 3000$ GeV.	48
3.15	Varying $m_{DM} = f = m_{Z'}/2$ and looking at the behaviour of RD.	49
3.16	Varying m_{π_c} (DM candidate) and looking at the percentage difference between masses of the stable and unstable dark pion for the SC.	50
3.17	A contour plot showing the RD for varying the percentage difference between the DM candidate and the diagonal Pion mediator (in percentage) of the SC and the value of f and m_{DM} .	50
4.1	The four kinds of fluxes, for four different cases in the parameter space.	54

4.2	The simulated photon fluxes for the two cases, SC and ZC.	56
A.1	Crossing symmetry for Compton scattering.	68
A.2	Feynman diagrams for the process releasing two photons.	69
A.3	Kinematics of the release of two dark photons process in the center of mass frame.	77

Chapter 1

Preliminaries

1.1 Introduction

One of the major challenges in physics is the search for missing matter in the universe, as suggested by many Astrophysical as well as Cosmological observations. It is believed that ordinary matter and radiation adds up to only 5% of all the matter energy content of the universe. The accelerated expansion of space necessitates the addition of a Dark Energy component in our Cosmological theories and calculation which forms an essential 68% of all matter-energy in the universe. This leads us to the hypothesised “extra” 27% of the remaining mass which we call Dark Matter. Dark Matter is a popular and a widely accepted solution to the problem, where it is believed that, the Standard Model of particle physics, which nicely describes all of the visible physics around us, can be extended to accommodate previously unaccounted, additional types of exotic matter. Studying dark matter comes with its own set of problems, one of which is that it does not interact with ordinary matter via the electromagnetic force. This means that it cannot be observed directly and must be inferred through its gravitational effects on visible matter. However, there are several indirect ways in which dark matter can be detected. As in most topics in science, a theory of Dark Matter must have a well developed and verifiable hypothesis of the same, which must be seen in the light of experimental results.

My focus here has been to learn about the field of Dark Matter (DM) Phenomenology in detail and contribute to research work in the same. The field of Beyond the Standard Model

physics presents us with a variety of potential new and interesting answers to unexplained problems in fundamental physics which would eventually help us understand the small-scale, as well as the large-scale structure of our universe better. Hence, as mentioned, an appropriate extension or re-modulation of our current understanding of the Standard Model with a Dark Matter description, providing results and predictions which can be verified to high accuracy is a very desirable aspect for physicists (which is very important, since we understand that Dark Matter as a concept was introduced specifically to explain experimental inconsistencies with the known theory). A possible solution to the inconsistencies of Astrophysical and Cosmological observations with our expectations, which has been explored for several years now, is the presence of DM which does not interact with ordinary matter via standard model interactions, or does so very weakly. Weakly Interacting Massive Particles (WIMP) interacting via the electroweak force (DM-SM) but with much weaker couplings than SM-SM and with no self-interactions (DM-DM), has been widely studied. For any theory of DM, cosmological predictions, direct and indirect detection observations must also be consistent. Several high-precision searches for various WIMPy DM models have been unable to see a reliable signal. In recent years, there has been growing interest in exploring the possibility of self-interacting dark matter (SIDM). This is a theoretical framework in which dark matter particles interact with each other through some unknown force. SIDM models offer a potential solution to several outstanding problems in the standard cold dark matter (CDM) model (say for instance, the ‘cusp-core’ problem). A possible solution to this, which we explore, is a hidden and confined DM sector with strong self-interaction of the particles, similar to mesons in QCD.

In the thesis, we start by understanding the underlying theory, concepts, calculation and computational techniques (as in the respective sections), and try to implement them in previously explored cases in literature. This showcases our understanding of the concepts for verifiable cases, after which, we move on to applying the wide range of knowledge gathered, in-order to build our own theory, and exploring the same.

The study of dark matter phenomenology is an active and exciting field of research that has the potential to revolutionize our understanding of the universe. With new observational and experimental techniques being developed all the time, we are poised to make significant progress in unraveling the mysteries of this elusive substance.

1.2 Astronomical Observations of Dark Matter

The Dark Matter (DM) detection techniques and observational evidences [1, 2] are well documented throughout astrophysics literature. Broadly speaking these are observational evidences either in the observed Cosmic Microwave Background (CMB), or in observing a surplus mass in galaxies and galaxy structures, leading to higher rotational velocities (observed through redshifts) than predicted by galactic models which takes into account only the matter visible through electromagnetic radiations (say for instance, estimating masses using X-Ray received from thermal Brehmstrahlung processes by hot-galactic media). For this purpose, gravitational lensing techniques come in handy in estimating the mass in a given region of a galaxy cluster. Various galactic model theories have been applied containing a variety of DM distribution schemes across the region spanned by the galaxy to search for a good candidate fit [3].

1.3 Overview of DM detection techniques

Direct Detection techniques are related to experiments and observations that try to look for existing DM in the universe by scattering them off a target. We do not have any description for cold dark matter in our current theory of the Standard Model (SM). The main requirements for a candidate are it being massive, non-relativistic, weakly-interacting and stable over billions of years. This rules out in general, charged particles, coloured particles and very light particles. It becomes necessary for us to look beyond the Standard Model of particle physics. It has been estimated that the local DM density must be of the order of $0.4 \text{ GeV}/\text{cm}^3$. For instance if DM is made up of particles of masses around 100 GeV, this results in about 4 particles/ m^3 . If we assume a model of a DM halo surrounding galaxies, Earth must come across many ($\sim 10^{13}$) DM particles per year. Dark matter interacts with standard matter via a scattering with the nucleons (or electrons) of the atoms present in such Direct Detection experiments. The recoil energy of nuclei are measured in order to measure the interactions of DM with ordinary matter, and to estimate the dark matter mass and the scattering cross section with nucleons, σ_N .

On the other hand, a more difficult detection process would be to produce and detect DM or novel particles produces in colliders at accelerator experiments. However multiple

limitations exist in such experiments based on various theoretical assumptions which makes such detections difficult. Clearly both Direct and collider constraints on the parameter space are important aspects while forming any new Beyond the Standard Model (BSM) theory.

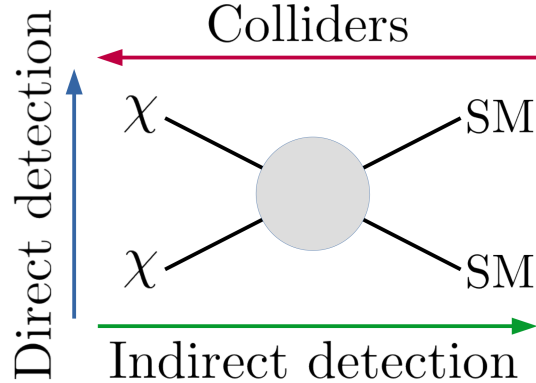


Figure 1.1: Schematic of the various detection possibilities for DM [1]

Indirect Detection techniques try to detect products of DM annihilation in DM dense astrophysical objects. Such annihilation processes might occur in the early universe, which also had high energy density with the potential to fuel them. Therefore, self consistency between early universe cosmology and current annihilation rates can imply the presence of Indirect Detection channels. A characteristic feature of such signals in general, is an anti-matter excess in the radiations observed from the source (as a consequence of DM annihilation and SM pair production). We can consequently, constrain the parameter space of a new DM theory further by imposing constraints learnt from such observations. The topic is explored further in [4.2] in the light of our work.

1.4 Scattering and Decays

Classically we describe scattering of particles as the change in trajectory of two interacting particles after a collision. We have the number of particles scattered per unit time in a given solid angle,

$$\frac{dn}{d\Omega} = F_i \sigma(\theta, \phi)$$

where F_i is the incident flux and σ is the cross-section of scattering. It depends on factors like kinetic energy, the impact parameter b of the incoming particles and the strength of the interaction. However dealing with sub-atomic particles necessitates quantum mechanics, and hence we turn to a description of quantum scattering cross-sections.

At sub-atomic levels, we can visualize particles associated with respective wave-functions and the fields related to force in the classical case as potentials which we can use in the Schrodinger equation (SE). For most asymptotic cases where we assume the incident particle on a potential as plane waves, and the scattered particles at the detectors ($r \rightarrow \infty$) as spherical waves (we can compute this by substituting the incident wave function for $V(r)=0$ at $r \rightarrow \infty$ in the SE).

We start by using Fermi's Golden Rule to construct a general expression for scattering and decays,

$$\Gamma_{fi} = 2\pi |T_{fi}|^2 \rho(E_f)$$

where, Γ_{fi} is the number of transitions per unit time from state i to f , T_{fi} as a transition probability matrix which is specific to the process, and ρ represents the density of states for the states that the particle can be found in. Here, we note that the state transition is the particle's initial to the particle's final state. Starting from,

$$\rho(E_f) = \left(\frac{dx}{dE} \right)_{E_f} = \int \frac{dx}{dE} \delta(E - E_f) dE$$

Therefore we can write Fermi's golden rule in terms of the four momenta of particles as,

$$\Gamma_{fi} = (2\pi)^4 \int |T_{fi}|^2 \delta(E - E_i) \delta^3(\mathbf{p} - \mathbf{p}_i) \frac{d^3 p_i}{(2\pi)^3}$$

$$T_{fi} = \langle f | T | i \rangle$$

$$T_{fi} = \langle \psi_{f1}, \psi_{f2} \dots | T | \psi_{i1}, \psi_{i2} \dots \rangle$$

With the f being the final states and i being the initial states of the interacting particles and T being the relevant interaction matrix (of the Hamiltonian) of the process. We can write a quantity M called the scattering amplitude which essentially has the relativistic correction $\phi = \sqrt{2E}\psi$ instead of ψ . This gives us a relation (we specify for a 2-2 scattering process)

$$T_{fi} = \frac{M_{fi}}{\sqrt{2E_{i1}2E_{i2}2E_{f1}2E_{f2}}}$$

For 2-2 scattering processes, we can show that the probability of interaction of one type of particle with another is given by

$$\Gamma = v\sigma$$

with v being the relative velocity between the particles. Therefore, substituting all of the above in the modified Fermi's rule, we shall have,

$$\sigma = \frac{(2\pi)^4}{(2\pi)^6 2E_1 2E_2 (v_1 + v_2)} \int |M_{fi}|^2 \delta\left(\sum_i E_i\right) \delta^3\left(\sum_i \mathbf{p}_i\right) \frac{d^3 p_3}{2E_3} \frac{d^3 p_4}{2E_4}$$

In the Centre of Mass (CoM) frame with $\sum_i \mathbf{p}_i = 0$, we can get to,

$$\sigma_{12} = \frac{1}{64\pi^2} \frac{|p_f^*|}{|p_i^*|} \int |M_{fi}|^2 d\Omega$$

where * represents the zero of the delta function, velocity is written as the ratio of momenta and energy, and with $s = (p_1 + p_2)^2$.

An even simpler derivation is the general expression for the decay rate of a particle into two others, calculated in the same spirit and given as,

$$\Gamma_{fi} = \frac{1}{32\pi^2} |p_1^*| \int |M_{fi}|^2 d\Omega$$

The decay rate, which also describes the probability per unit time, of having the initial state of a single particle, decay into multiple new particles can therefore also be derived using a quantum picture.

This therefore brings us to the simple conclusion of the relation of the decay rates to the interaction between the particles at a vertex being proportional to each other in a crude sense.

Chapter 2

Calculating Dark Matter Density

2.1 Thermal Relic density and Freeze-out

The minimal idea of how to estimate the DM density comes from the idea of how a thermal bath of all particles in the early universe behaves in an expanding universe. Assuming that all particles are in thermal equilibrium in the early universe, the new particles can have the distribution functions of Fermi-Dirac for fermions and of Bose-Einstein for bosons which is given by,

$$f_i(E_i, \mu, T) = \frac{g_i}{\exp\left(\frac{E_i - \mu}{k_B T} \pm 1\right)} \quad (2.1)$$

where the + sign is for fermions and – for bosons, g_i is the degeneracy (degrees of freedom), μ being the chemical potential and k_B being the Boltzmann constant. Such distributions in the primordial soup of the early universe, where the temperatures are very high simplify to the Maxwell-Boltzmann distribution for cases where the interactions between particles are weak and the chemical potential is negligible. Whilst the particles are in thermal equilibrium with the plasma with a common temperature, the distributions are driven only by the temperature. However, as the universe expands, and the temperature decreases, not only does the energy carried by particles for each collision reduce, the distances between particles in the plasma, on an average increases, which limits the rate of interaction. The equilibrium can hence be broken, and the unstable particles decay and the stable ones undergo a “Freeze-out”. We introduce the concept of Relic Density (RD) which refers to the

density of DM particles in the universe at the time of “Freeze out” (Thermal Relic density) (“Freeze in” in the case of non thermal DM density)[\[4\]](#). In the case of Thermal DM and its consequent Thermal RD, the DM particles which we seek to know more about are in thermal equilibrium in the early stages. Since the stable particles do not decay, their number density is frozen to a constant owing to their low interaction rates. Consequently the number density of stable particles decreases as a^{-3} .

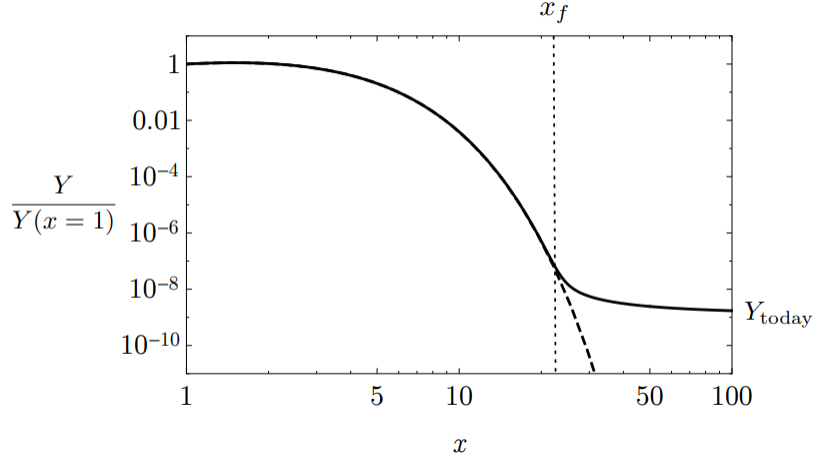


Figure 2.1: An illustration of the DM Relic density before and after thermal Freeze-out (z_f) of WIMP, [\[3\]](#). Here Y refers to scaled value of the relic density, which follows the curve Y_{eq} up till Freeze-out.

2.1.1 Explanation for DM Relic density [\[3\]](#)

We look closely into the Freeze-out scenario and try to quantify the Relic Density of DM. We follow the evolution of the inelastic scattering process with time using the Boltzmann equation. We have, the number density of a given particle is related to its phase-space density, $f(E,t)$,

$$n = g \int f(E, t) \frac{d^3p}{(2\pi)^3} \quad (2.2)$$

where g is the number of spin degrees of freedom of the particle. After Freeze-out, the DM is no longer in chemical equilibrium i.e. through inelastic scattering with another DM particle leading to two standard model particles, but it remains in thermal equilibrium with the surrounding plasma via the elastic interactions. We look at two sides of the Freeze-out

equation separately. Putting in a simple way, the LHS looks at the change in number density of the DM particles with time. To take into account the expansion of the universe, we scale the n term in the LHS by a factor of $\frac{1}{a^3}$, to eventually give us,

$$\frac{d}{a^3 dt} na^3 = \frac{dn}{dt} + 3Hn \quad (2.3)$$

Where H is the Hubble's constant and equal to $\frac{\dot{a}}{a}$, and a is the cosmological Scale-factor.

The RHS, shows the change in the number of DM particles produced/ annihilated using the difference in the forward and reverse reaction rates as,

$$\begin{aligned} & -\Sigma_{spins} \int (f_1 f_2 (1 \pm f_3) (1 \pm f_4) |M_{1,2 \rightarrow 3,4}|^2 - f_3 f_4 (1 \pm f_1) (1 \pm f_2) |M_{3,4 \rightarrow 1,2}|^2) \\ & \cdot (2\pi)^4 \delta^4(p_1 + p_2 - p_3 - p_4) d\Pi_1 d\Pi_2 d\Pi_3 d\Pi_4 \end{aligned} \quad (2.4)$$

In the above equation, f_i and g_i are the phase-space densities and spin degrees of freedom, respectively, for particle i , and $M_{x \rightarrow y}$ is the scattering amplitude for the reaction $x \rightarrow y$. Terms like, $(1 \pm f)$ are used to represent Pauli blocking and Bose enhancement; minus sign for fermions and plus signs for bosons. These terms are based on the logic that it is easier for a boson to transition to a state that already contains a boson and harder for a fermion to transition into a state that already contains a fermion. The four dimensional delta term limits the possible values of the momenta of the particles to those allowed by the momentum conservation only in the momentum space. The last four differentials are the three dimensional phase space integration factors, given by-

$$d\Pi_i = \frac{d^3 p_i}{(2\pi)^3 E_i}$$

We can make the following assumptions to simplify our calculations-

- The phase-space distributions take on the Fermi-Dirac or Bose-Einstein forms, due to kinetic equilibrium.

- The temperature of each species satisfies,

$$T_i \ll E_i - \mu_i$$

where μ_i is its chemical potential, so that they follow the Maxwell-Boltzmann distribution. In this case, $(1 \pm f)$ approximately equals 1.

- The visible sector particles involved in the interactions are in thermal equilibrium with the photon bath.

We define a quantity, Møller velocity as,

$$(v_{Ml}) = \frac{\sqrt{(p_i \cdot p_j)^2 - (m_i \cdot m_j)^2}}{E_i E_j} \quad (2.5)$$

Consequently we can re-write the RHS of our equation as,

$$- \int (v_{Ml})_{12} dn_1 dn_2 (v_{Ml})_{34} dn_3 dn_4 \quad (2.6)$$

where, σ_{ij} is the cross section matrix for the scattering process. The Møller velocity is Lorentz invariant, whereas $v_{rel} n_i n_j$, the relative velocity for relativistic processes is not. When the DM is also in equilibrium with the Standard Model final states,

$$\langle \sigma v \rangle_{12} n_{eq}^2 = \langle \sigma v \rangle_{34} n_3^{eq} n_4^{eq} \quad (2.7)$$

Consequently, The Boltzmann equation can be reduced to,

$$\dot{n} + 3Hn = \langle \sigma v \rangle (n_{eq}^2 - n^2) \quad (2.8)$$

i.e. we express entirely in terms of DM cross-sections and number densities. n_{eq} accounts for the creation of the DM, χ through the inverse process and n accounts for the depletion of

DM particles χ through annihilation. Given that the universe is expanding, we can scale the DM number density by a factor s , the entropy density of the universe, to define, $Y = n/s$. Therefore we can study the evolution of DM number density without worrying about it's reduction due to expansion effects and only due to the interactions of the DM with particles that are in thermal equilibrium with the photon bath. Therefore our equation is modified as,

$$\frac{dY}{dt} = \langle\sigma v\rangle s(Y_{eq}^2 - Y^2) \quad (2.9)$$

$$\frac{dY}{dx} = \frac{-xs\langle\sigma v\rangle}{H(m)}(Y^2 - Y_{eq}^2) \quad (2.10)$$

where $x = m/T$ is the re-scaled time variable in which m is the mass of the DM. We have also used the fact that sa^3 is constant to get the relation that $\dot{s} = 3sH$ in the above expressions to get s instead of H . To be more elaborate, we write the time derivative of Y as a product of the re-scaled time derivative of Y and dx/dt . We have used a simple logic that, the photon temperature is inversely proportional to its wavelength, which scales with a .

$$\frac{dY}{dx} \frac{dx}{dt} = \langle\sigma v\rangle s(Y_{eq}^2 - Y^2) \quad (2.11)$$

using, $x = \frac{m}{T}$, T as K/a and $H(x)$ in terms of $a(x)$ and it's time derivative, we can write-

$$\frac{d}{dt} \left(\frac{m}{T} \right) = m \frac{d}{dt} \frac{a}{K} = \frac{ma}{K} \cdot \frac{\dot{a}}{a} = \frac{mH(x)}{T} = H(x)x \quad (2.12)$$

Here Y is therefore the DM number density re-scaled to remove the effects of the universe's expansion (related to RD as, $Y = 2.8 \cdot 10^{-8}$ RD). Therefore, the changes in Y as in the Boltzmann equation are strictly from interactions of the DM with states present in thermal equilibrium with the photon bath. No analytical solution exists for the expression above and one must rely on numerical methods.

We have been looking at a specific DM model which shapes the eventual DM RD observed today. We can explore the parameter space of each constructed model and the corresponding RD to learn more about the constraints from observed quantities which we must worry about. In the following sections, we will be looking at the make-up and results of two tried and tested Freeze-out models using a program “MadDM” [5], and analysing the data.

2.2 Simplified dark matter model with spin-0 mediator

Here we look at simple extensions of the Standard model lagrangian. In our case, in addition to particles and terms present in L_{SM} , we introduce fermionic Dark Matter, and a singlet scalar (s-channel) mediator belonging to the dark sector and connecting the SM and the dark sectors. Consequently, the strengths of the interactions between the Dirac DM and the singlet scalar (denoted by Y_0), and similarly, the SM particles and the scalar are dependent on their masses. We referred to [6] for a general impression of how to include extra scalar fields in our Lagrangian.

2.2.1 General Observations

- The more probable (bigger cross-section), the forward reaction (corresponding vertex strength) is, lower will be the predicted RD (observed value= 0.112) and vice versa. This would mean that more and more DM particles annihilate into the scalar Y_0 which in turn can pair produce SM particles, thus carrying the energy density from the hidden sector to the SM sector. There must exist an equilibrium for this process for some values of couplings for SM- Y_0 and DM- Y_0 (i.e. for a ratio of the two numbers). If the ratio of DM- Y_0 to SM- Y_0 is more than this value, the forward reaction will be favoured and the RD is lowered.
- The observed DM relic density is 0.112. Any scenario leading to a lower RD is called under-abundant and a higher RD is called over-abundant. It’s a neat task to scan the parameter space generated by our model and realise the observational constraints in it.
- In this model, mass of dirac DM, mass of additional scalar, and couplings between the scalar field and the particles, happen to be reasonable parameters.

- A basic Feynman diagram for the general process has been provided. S refers to the singlet scalar. The motivation behind the addition of such a particle in an extended theory is that, it provides an outlet for generating DM masses in a simplified hidden sector.

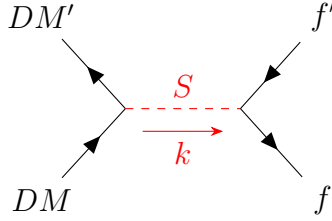


Figure 2.2: Feynman diagram for the process

2.2.2 Hidden sector contribution to the Lagrangian

We group the Lagrangian into two segments.

$$L_{X_D}^{Y_0} = \bar{X}_D (g_{X_D}^s + i g_{X_D}^p \gamma_5) X_D Y_0 \quad (2.13)$$

$$L_{SM}^{Y_0} = \sum_{i,j} \left[\bar{d}_i \frac{y_{ij}^d}{\sqrt{2}} (g_{d_{ij}}^s + i g_{d_{ij}}^p \gamma_5) d_j + \bar{u}_i \frac{y_{ij}^u}{\sqrt{2}} (g_{u_{ij}}^s + i g_{u_{ij}}^p \gamma_5) u_j \right] Y_0 \quad (2.14)$$

2.2.3 Relic Density over parameter space

We present the results of the parameter space for the RD. In all of the figures of [2.3](#), we must keep our sight around the 10^{-1} contour line to guide us as that is close to the observed RD value of 0.11. The coupling-coupling parameter space figure has quite a predictable behaviour, with the RD decreasing, roughly linearly, as we increase either of the coupling values. The (coupling of DM to scalar- DM mass) plot also has a predictable behaviour, with a minima in the predicted RD lying around the region where the DM mass is about half of the mediator mass, owing to on-shell resonance effects. In our case, the minima also lies around the 0.1 contour line. The RD increases significantly as we go away from the sweet

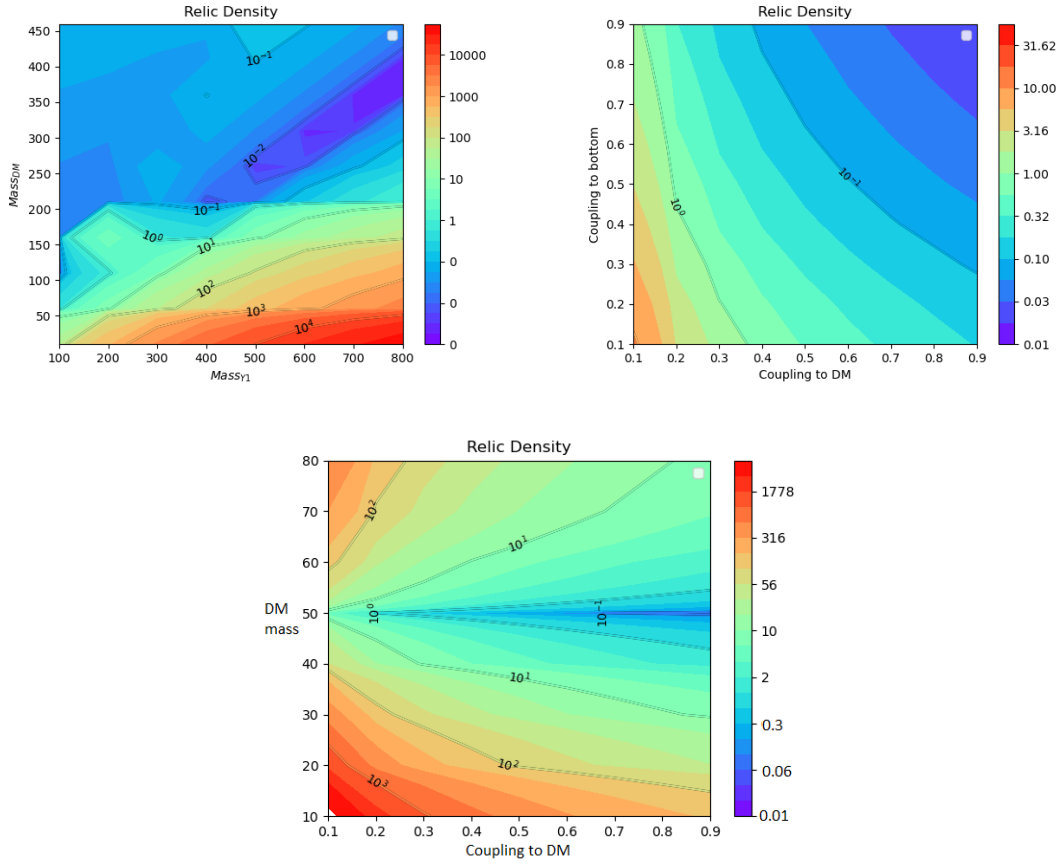


Figure 2.3: Exploring the value of the RD over the parameter space for the spin-0 mediator model. RD for (top left) varying mass of DM and scalar mediator Y_0 , (top right) varying couplings of Y_0 , (bottom) varying mass of DM and coupling of Y_0 to DM; All above masses have been represented in GeV.

spot, in either direction. As compared to the change in DM mass, the change in coupling value from 0.1 to 1 has a less pronounced effect on the RD. As the coupling of Y_0 to DM increases, the forward reaction of the already described s-channel process increases, leaving less energy in the dark sector and a lower RD. A plot capturing the RD in the parameter space of changing masses and fixed couplings is also provided in figure 2.3 for reference. In the first figure, we keep all the Y_0 coupling values at 1, varying the tun-able mass parameters. In the second figure, the DM mass is also kept fixed at 50 GeV and only the couplings, which contribute sufficiently to the RD are varied. In the third figure, all Y_0 to quark couplings are kept at 0.5, whereas the DM mass is varied. Additionally, for both the second and third figure, we explore the parameter space of the RD for fixed spin-0 mediator mass 100 GeV.

2.3 Simplified dark matter model with spin 1 mediator

Once again we look at another simple extension of the SM Lagrangian. Here, in addition to particles and terms present in L_{SM} , we introduce fermionic DM, and a vector (s-channel) mediator belonging to the dark sector and connecting the SM and the dark sectors. The strengths of the interactions between the Dirac DM and the singlet scalar (denoted by Y_0), and similarly, the SM particles and the mediator are no longer dependent on their masses. For DM candidates heavier than a collection of quarks, all the quarks channels contribute equally to the eventual RD. A singlet scalar field does exist in the Lagrangian, but only to give mass to the particles in the dark sector, and not as a mediator. It doesn't interact with the SM particles. However we now have dark vector-SM, and dark vector-Dirac DM couplings as new sets of parameters along with the mass parameters. General observations are the same as in the previous section.

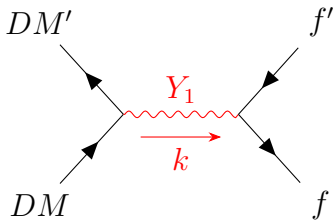


Figure 2.4: Feynman diagram for the process

2.3.1 Hidden Sector Contribution to the Lagrangian

Similar to the previous case, we write the Lagrangian as,

$$L_{X_D}^{Y_1} = \bar{X}_D (g_{X_D}^V + i g_{X_D}^A \gamma_5) X_D Y_1^\mu \quad (2.15)$$

$$L_{SM}^{Y_1} = \sum_{i,j} \left[\bar{d}_i \gamma_\mu (g_{d_{ij}}^V + i g_{d_{ij}}^A \gamma_5) d_j + \bar{u}_i \gamma^\mu (g_{u_{ij}}^V + i g_{u_{ij}}^A \gamma_5) u_j \right] Y_0 \quad (2.16)$$

where X_D is the Dirac fermion, d and u denote down and up type quarks, respectively, $(i, j = 1, 2, 3)$ are flavour indices, and $g^{V/A}$ are the vector/axial-vector couplings of DM and

quarks. We can get the pure vector and pure axial-vector mediator scenarios by setting the parameters values appropriately.

2.3.2 Relic Density over parameter space

Upon comparing the behaviour taken up by the RD in the spin-1 mediator case to that of the spin-0 mediator, we recognize the similarities in certain aspects (after-all the overall mechanism remains the same (s-channel dominated energy transfer) and only the nature of the mediator changes from a scalar to a vector one.

- In the first image of figure [2.5](#), once again, the minima for RD lies roughly around DM mass equaling half of the mediator mass, along with other similar features. However, unlike before, it doesn't coincide with the observed RD of 0.11. The 10^{-1} contour largely lies between DM masses of 200 GeV-400 GeV for the coupling range of 0.1 - 0.9 (i.e. about 3/10 of the mediator mass on average).
- The DM mass- Y_1 mass plot has a RD minima along the diagonal as can be seen, quite similar to the spin-0 case. The area which interests us, once again, is the 10^{-1} contour line which heavily depends on the mass of Y_1 than the DM mass. This is expected in light of what we observed in the DM coupling-mass plot (observed RD lying around 3/10 of mediator mass).
- In figure [2.6](#), we see how RD changes with changing the mediator coupling, both on the SM side (for all particles) and the DM side. As we can see, the change in RD along either axis is roughly symmetric hinting towards equal weight-age towards the RD. For the DM mass equal to 4 GeV case the 10^{-1} contour occurs at smaller coupling values whereas for the DM mass equal to 1 GeV case it occurs only at higher coupling values.

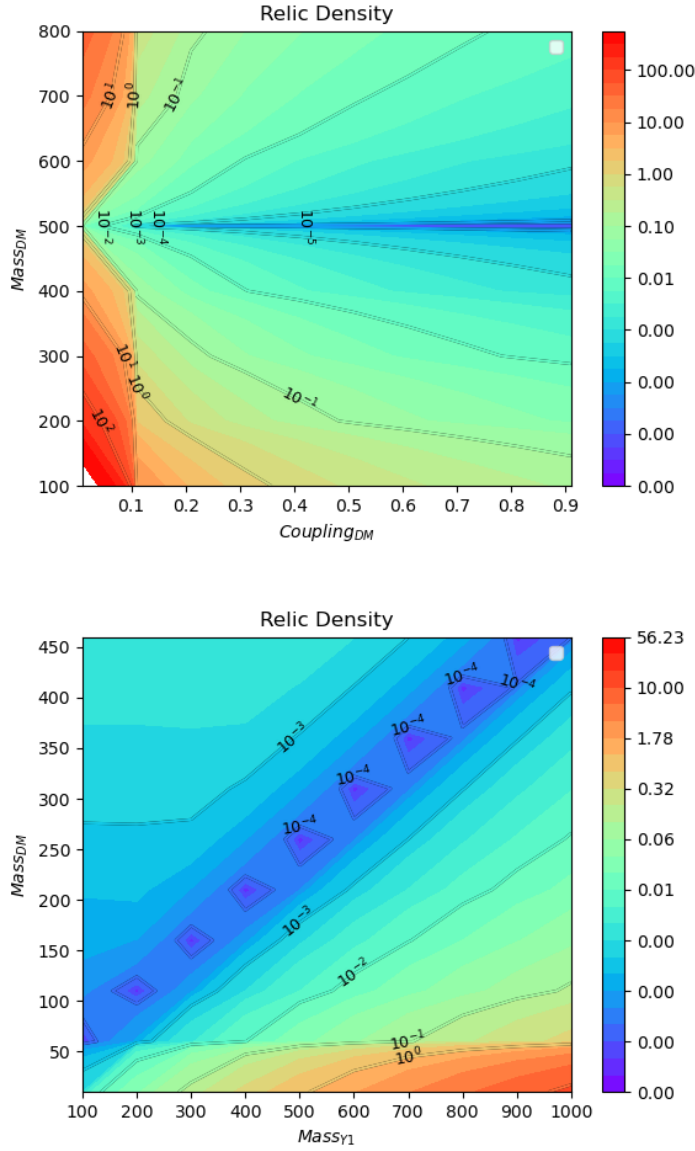


Figure 2.5: Exploring the value of RD over the parameter space for Spin-1 Mediator: The figure on the top shows the variation as a function of DM mass and DM coupling to the vector mediator, for a fixed mediator mass of 1000 GeV. The second figure looks at the variation as a function of the two tun-able mass parameters for fixed coupling values for the DM and SM particles to the mediator. The “island” like minima zones are a result of the granularity of our parameter scan. Had they been continuous, or if we had smaller step sizes, we should have encountered a continuous band across the diagonal. All masses are presented in GeV.

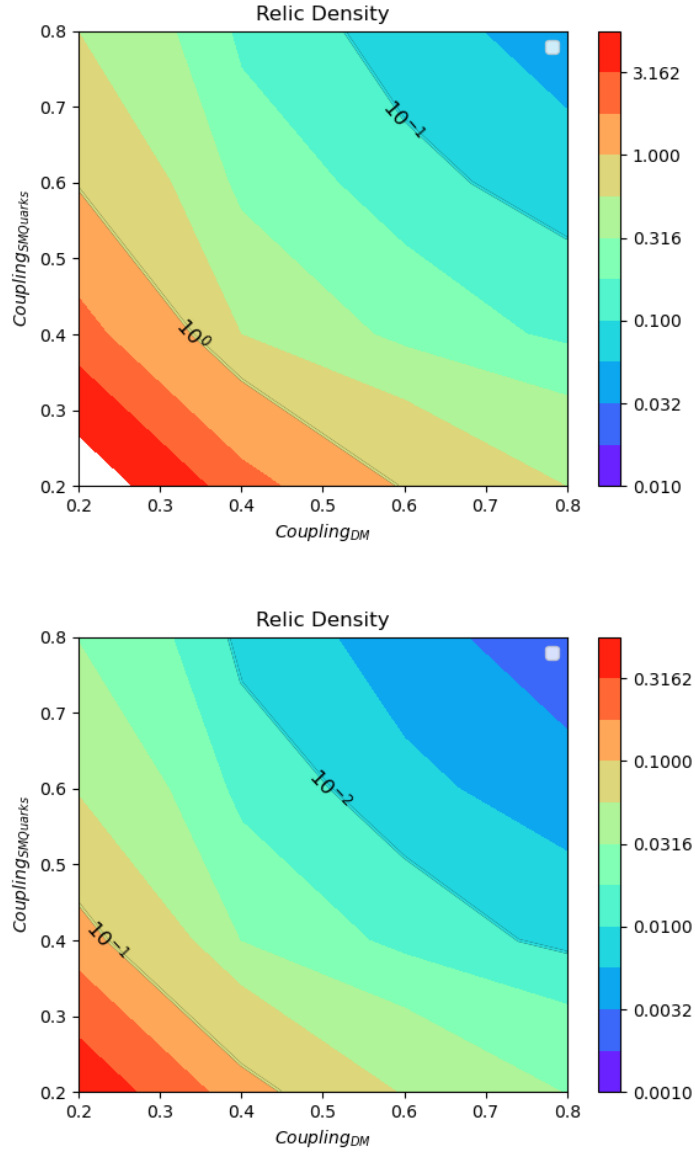


Figure 2.6: Exploring the Relic Density over the parameter space: Looking at RD whilst changing couplings of the vector mediator Y_1 to DM and SM quarks. The first figure is for DM mass 1 GeV and the second figure is for DM mass 4 GeV for a mediator mass of 100 GeV.

2.4 The Freeze-in mechanism and the FIMPs

Freeze-out has been studied in detail over many decades [3, 1, 7]. On the other hand, an assumption that DM does not exist in the primordial soup but is created later, is an alternate hypothesis that is explored in the Freeze-in paradigm [4].

In the Freeze-in mechanism, the DM density stems from a DM creation process instead of resulting from the thermal Freeze-out of the DM annihilation process, for example through annihilation into DM particles via s-channel ($AA \rightarrow \text{DM DM}$) or a decay process giving atleast one DM particle in the process ($A \rightarrow \text{DM } B$). Such processes, assumed to already be out of thermal equilibrium, freeze when the production rate gets Boltzmann suppressed as we had seen earlier; i.e. when the kinematics of the reaction fueled by the temperature falls below the masses of A or DM depending on the reaction. Like in Freeze-out the number of particles produced depends only on the masses and couplings involved in the DM creation process. As mentioned, the Freeze-in mechanism requires weaker couplings to the standard model particles than WIMPs, and introduce particles called Feebly Interacting Massive Particles (FIMP). To start with, the FIMPs were de-coupled from the primordial plasma, and may have only been created in limited amounts through the decay of the primordial fields. However, even though they interacted feebly with the plasma, these interactions still caused the production of more FIMPs and increased their concentration until the temperature of the plasma became too low for it to be kinematically feasible to produce them any further. In contrast, Freeze-out scenarios do not rely on any such assumptions about the initial creation of these particles since they are assumed to have been in thermal equilibrium from the start.

The substantially weak couplings associated with FIMPs (approximately 8-10 orders lesser than WIMP) makes it difficult to detect via direct or indirect detection of the s channel type processes at colliders. Therefore we understand that the DM essentially lies in some dark (or hidden) sector that is feebly coupled to the visible sector. The full hidden sector (the parts not included in the SM Lagrangian) Lagrangian can be written as

$$\mathcal{L} = \mathcal{L}_{SM} + \bar{\psi}'(iD' + m_{\psi})\psi' \quad (2.17)$$

here, the second term represents the hidden sector with weak coupling.

The A particles can be abundantly produced at colliders if A has substantial coupling

to the SM particles in the visible sector. It is to be noted that, A could be either, a known SM particle or a new hypothetical particle. However, a new particle is likely to be long-lived due to its feeble couplings.

Another possibility is that of direct detection (the A - A annihilation reaction). Here the A particle is a SM particle, which would mean that the predicted DM density depends only on the DM particle mass, on the interaction with the connector particle A and on any interaction which may be important within the hidden sector.

2.4.1 Freeze-in via dark photons

The dark photon model involves QED-like interactions between a new gauge boson γ' and a DM particle in the hidden sector that is charged under this new interaction. It involves in addition to the SM sector, new fermions which are assumed to be charged under a new $U(1)'$ gauge symmetry. Thus, in principle, in a most general but simple model, the Lagrangian should have the SM current, the light mediator or dark photon coupling with the fermionic SM current, a term containing the dark fermion and dark photon, the dark fermion coupling with the SM terms and a kinetic mixing term as we will see in figure [2.7](#). The need for the presence of each of these terms should be specific to the relative coupling strengths used in our model. In the case of the study, if the kinetic mixing and hidden sector terms are feeble, then we can simply determine the density of dark matter by counting the number of dark matter particles created through the connector, i.e. the Freeze-in scenario, and ignore the hidden sector interaction with the SM sector. However, if either one or both of the interactions are stronger, we must take into account the effect of thermalization in both the visible and dark sectors on the DM density.

The Lagrangian used for the model-

$$\mathcal{L} = \mathcal{L}_{SM} + \bar{\psi}'(iD' + m_{\psi})\psi'$$

We can add The Kinetic mixing portal, to the above model, which looks like-

$$\mathcal{L} \ni -\frac{\epsilon}{2}F^{\mu\nu}{}_Y F'_{\mu\nu} \tag{2.18}$$

We have the following couplings to the SM and DM currents,

$$L \ni -e_{EM} J_{EM}^\mu \gamma_\mu + e' \frac{\epsilon \cos \theta_\epsilon}{\sqrt{1 - \epsilon^2}} J_{DM}^\mu \gamma_\mu - e' J_{DM}^\mu \gamma'_\mu - e' \frac{\epsilon \sin \theta_\epsilon}{\sqrt{1 - \epsilon^2}} J_{DM}^\mu Z_\mu - g \frac{\cos \theta_W}{\cos \theta_\epsilon} J_Z^\mu Z_\mu \quad (2.19)$$

with J_{SM}^μ and J_{DM}^μ corresponding to the $U(1)_{em}$ and $U(1)'$ currents, θ_W is the Weinberg angle, ϵ is a quantity much smaller than 1, see appendix [A.1](#) and where we have defined,

$$e_{EM} = \frac{e}{\sqrt{1 - \epsilon^2 \cos^2 \theta_W}}$$

The dominant process for the transfer of energy from the visible sector to the hidden sector is through the creation of DM pairs, via the s-channel. The relative probability of encountering one of the contribution (and hence considering them in our calculations) depends on various factors.

For the case where we ignore Z acting as a mediator, we look at the case of $m_{DM} > m_Z/2$. For $m_{DM} < 1$ GeV also, the process via the Z boson can be ignored as the process via the γ is enhanced at low temperatures. For the corresponding intermediate mass range it is more convenient to express all Boltzmann equations directly in terms of the decay width.

2.4.2 The Boltzmann equation

Considering all the dominant processes we can approximate to ignore certain process. We summarise as follows.

From figure [2.7](#), we can see processes of the first kind as above are the most important in the Boltzmann equation for terms including energy transfer. The last term, is also included as the hidden sector interaction. The complete Boltzmann equation looks like-

$$szH \frac{dY}{dz} = \sum_i \gamma_{connect}^i \left(1 - \frac{Y^2}{Y_{eq}^2(T)} \right) + \gamma_{HS} \left(1 - \frac{Y^2}{Y_{eq}^2(T')} \right) \quad (2.20)$$

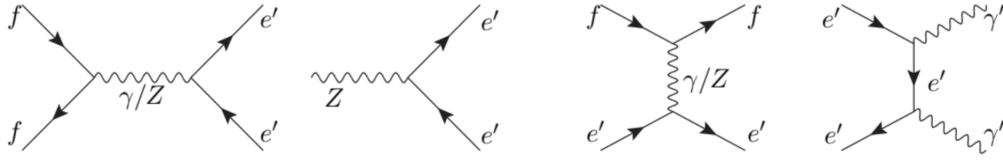


Figure 2.7: In the figure, we see Feynman diagrams of the processes for the production of DM and thermalization of the hidden sector (HS). We work in the basis such that hidden photons only couple to DM and not SM degrees of freedom. The first figure with the s-channel mediator is our dominant process. The last figure on the extreme right includes energy being carried away from the HS but no energy transfer to the visible sector. The third figure with the t-channel has experimentally low contribution to our calculations.

with s the entropy density, H the Hubble constant and Y the DM number density to entropy density ratio, $Y = \frac{n_e}{s}$. z is some alternate description of the time variable written in terms of H . The first one, $Y_{eq}(T)$, parametrizes the number of SM particles participating in the $SM_i SM_i \rightarrow DM DM$ processes. The second one, $Y_{eq}(T')$, parametrizes the number of γ' which participate in the dark fermion- dark photon interaction as shown above. Therefore the Y_{eq} 's correspond to their respective equilibrium number density n_{eq} 's in the subsequent reactions. Note that the γ 's in equation [2.20](#) do not represent “photons” but rather is a scaled reaction probability rate, $\gamma = \Gamma n_{eq}$. Recall that the reaction probability rate can be written for a specific reaction with the knowledge of the type of interaction, interacting particles, Cross section amplitude M and the relativistic four-momentum phase space integral terms.

Equivalently, we can also write in terms of cross sections,

$$z \frac{H dY}{s dz} = \sum_i \langle \sigma_{connect} v \rangle_i (Y_{eq}^2(T) - Y^2) + \langle \sigma_{HS} v \rangle (Y_{eq}^2(T') - Y^2) \quad (2.21)$$

Now based on the relative values of T and T' , there can be two possible scenarios.

a) If the DM particles do not thermalize with the dark photons, which happens if the terms specifying the coupling strengths of the hidden sector terms (their interactions to the visible sector) are small, the Boltzmann equation for the DM abundance simplifies. It is the case when $T \gg T'$; the dark fermion to dark photon reaction doesn't reach equilibrium.

Instead the temperature is way higher, as a result of which, the majority of the dark fermions annihilates into dark photons, allowing us to get rid of one term in our modified equation.

$$szH \frac{dY}{dz} = \sum_i \gamma_{connect}^i \left(1 - \frac{Y^2}{Y_{eq}^2(T)} \right) \quad (2.22)$$

Therefore, the number of DM particles is based on the balance between DM pair creation from SM particles and vice-versa.

b) If the hidden sector thermalizes for some $T' \leq T$, we must perform all the necessary calculations for the second term as well. We will need T as a function of T' . For this purpose, we need the hidden sector energy density ρ' as a function of T . We can use the cosmological Scale-factor a to express the energy density as some power law of T . The energy density transferred to the hidden sector by a process of the form $12 \rightarrow 34$ is given by the following Boltzmann equation.

$$\frac{d\rho'}{dt} + 3H(\rho' + P') = \int \prod_{i=1}^4 d^3\vec{p}_i \cdot g_i f_1(\vec{p}_1) f_2(\vec{p}_2) |iM|^2 (2\pi)^4 \delta^{(4)}(p_1 + p_2 - p_3 - p_4) \Delta E_{tr} \quad (2.23)$$

In short, the RHS in the above expression accounts for the energy transfer from the visible sector to the hidden sector via the $SM_i SM_i \rightarrow DMDM$, 2-2 scattering process as we have discussed.

The LHS however captures, the total change in energy density which the hidden sector undergoes, as a result of the above process. Here, ρ' accounts for the energy density of DM in the universe. Here is a brief work out of the LHS-

Combining the two Friedmann equations we can get to a result,

$$\frac{d(\rho(t)a^3)}{da} + 3p(t)a^2 = 0 \quad (2.24)$$

Expanding this we get,

$$\frac{d\rho}{da} = \frac{-3(\rho + P)}{a} \quad (2.25)$$

$$\delta\rho = -3(P + \rho)\delta\ln a \quad (2.26)$$

$$\frac{d\rho}{dt} + 3H(\rho + P) = 0 \quad (2.27)$$

This expression therefore depicts, the change in energy density. It also relates the same energy density to the Scale-factor which can then be used to relate ρ' to T as required. Everything included, we shall have the complete expression relating the visible sector energy density, and T to ρ' , we have-

$$\frac{d(\frac{\rho'}{\rho})}{dT} = -\frac{g_1 g_2}{H(T)T\rho 32\pi^4} \int ds \cdot \sigma(s)(s - 4m^2) s T K_2 \left(\frac{\sqrt{s}}{T} \right) \quad (2.28)$$

see [4] Appendix C

Comparing the LHS of equations [2.23] and [2.28] for the same RHS (the modification of the RHS in equation [2.23] to that of [2.28] can be seen in Appendix C of [4]) we essentially need to show that,

$$\frac{\partial\rho'}{\partial t} + 4H\rho' = \frac{\partial\rho'}{\partial T} H(T)T\rho \quad (2.29)$$

with the need to change variables from time coordinates to temperature coordinates.

Expanding the RHS of the above equation [2.29],

$$\left(\frac{\partial\rho'}{\rho\partial T} - \frac{\rho'\partial\rho}{\rho^2\partial T} \right) H(T)T\rho \quad (2.30)$$

Using equation of state corresponding to a radiation dominated universe and differentiating both sides with respect to T,

$$\frac{\partial \rho}{\partial T} = -4\rho \frac{\partial t \partial \ln a}{\partial T \partial t} \quad (2.31)$$

$$\frac{\partial \rho}{\partial T} = -4H\rho \frac{\partial t}{\partial T} \quad (2.32)$$

Therefore upon substituting equation [2.32](#) in equation [2.30](#), we see that, $H(T)$ must be equivalent to $\frac{\partial}{\partial t}$, which is exactly the case in an expanding universe, where we need to take into account, the expansion coefficient a and its change with time. Hence,

$$\frac{\dot{a}(t)}{a} T = H(T)T \approx \frac{\partial}{\partial t} T \quad (2.33)$$

We show the detailed calculation of the scattering amplitudes and cross-sections, which are to be put in a Boltzmann equation solver in Appendix [A.1](#).

2.4.3 Parameters for Freeze-in

We now briefly, look at the significance of the connector parameter κ ($= \epsilon \sqrt{\alpha/\alpha'}$, contains coupling parameter related to both the visible and hidden sector), and Hidden Sector coupling term α' to see how varying parameters affect the make up of the model. In the Boltzmann equation calculations of equation [2.21](#), we saw contributions from both the connector terms, and the exclusively hidden sector term. If we are to make qualitative categories for the contribution of the different terms,

- Removal of the HS term essentially removes the contribution from the hidden sector process, $DM DM \rightarrow \gamma \gamma$, whose cross section depends on the parameter α' . Hence for low enough values of α' and κ , all we are left with is an expression which looks like,

$$\frac{dY}{dT} = \frac{-\gamma_{connect}}{TH(T)s} \quad (2.34)$$

i.e. we ignore the last three terms of the equation completely, this as we discussed before, corresponds to the Freeze-in scenario, where we don't have any interactions to

thermalize the DM particles. Therefore typically, since the DM particles are already frozen out, the energy density increases with decreasing temperature as the connector processes converts SM particles into DM ones. Thereafter the relic density hits a plateau as discussed in section 2.

- With an increase in either κ or α' , the other terms i.e. the HS terms and the connector terms also start having a sizeable contribution to the RD. For instance, if we are to increase ϵ keeping α' constant, we include the second term of equation 2.21, and if both κ and α' were to increase, the HS terms also contribute. This case is also called the re-annihilation regime.

We reproduced the Dark matter Relic Density as a function of z ($= m_{DM}/T$), in the simplest, Freeze-in scenario, discussed previously, as an exercise in figure 2.8.

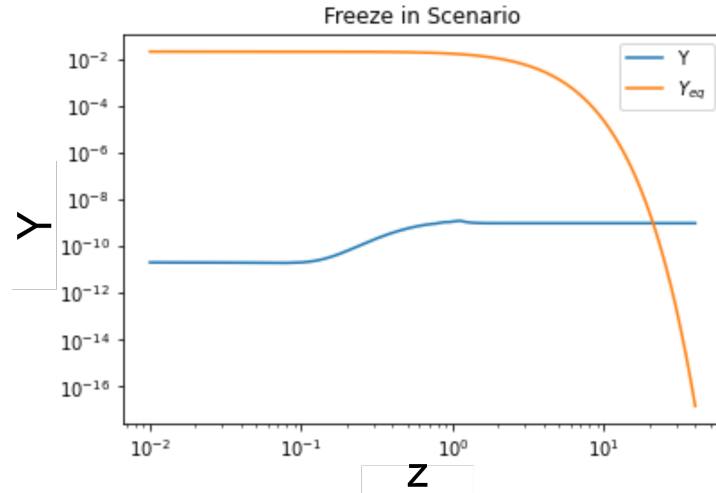


Figure 2.8: Calculated DM density Y , for the freeze-in scenario, along with the expected equilibrium density Y_{eq} , which represents a case of DM being in thermal contact with its surrounding plasma, in the early universe.

Chapter 3

Strongly Interacting Dark Matter

With the backbone of a hidden sector connected to the SM sector via a vector mediator, we proceed to modify the dark sector to include confined composite particles composed of "dark quarks". One can refer to similar ideas found in [8, 9, 10, 11]. We also referred to [12] for some theoretical insight of vector mediators in DM theories which we would be using.

3.1 A model of Dark Pions

We start with drawing inspiration from the SM, and what we observe around us. Our current understanding of the SM does classify all particles and force mediators using, fermions and bosons. At low energy scales, which are relevant for most of the physics we study, most of the matter around us, manifest and make their presence felt as bound states of quarks such as mesons and hadrons. Such stable states of matter allow the rich nuclear chemistry and an interactive particle zoo which we see around us, which further allows an even richer atomic chemistry when we speak of even lower energy physics. It should be a good guess to envisage a similar picture of the hidden sector, even if not as rich with the same variety of particles in the SM.

In our model, we propose that early universe cosmology, which deals with extremely high temperature and thus very high energy physics, involves the presence of 'strongly' charged fermionic DM with two flavours (we shall be calling them \tilde{d}_1 and \tilde{d}_2 going forward). They are

responsible for the cosmological results at extremely early times (which might potentially be verified in the future when we learn to harness multimessenger astronomy and GW analysis even better). As the universe cools down and the DM (along with other SM particles) particles lose kinetic energy. This leads to confined states of DM, much like what we see in case of mesons like pions, or hadrons like the proton. This analogy which we can draw with the SM mesons also enables us to borrow the mathematical machinery corresponding to it.

We have an additional $SU(3)'$ group, similar to the $SU(3)$ gauge group used for QCD. Only the dark fermions however are charged under the new gauge symmetry. Accordingly we also introduce the force mediator, dark gluons and a new index called dark colour (three types), carried by the dark fermions and dark gluons. This gives rise to the so called ‘strong interaction’ of the dark sector.

After confinement, the DM of this theory consists of a stable dark pion comprising of bound states of the dark fermions similar to charged pions in SM. We have, $\tilde{d}_1\tilde{d}_2 = \pi_c$ and $\tilde{d}_2\tilde{d}_1 = \pi_c^\dagger$. We refer to these as cross dark pions.

The diagonal bound states π_d have a dark fermion along with its own anti-particle, and is therefore unstable. It easily decays into SM particles, via some Z' . We have a four-vertex $\pi_c\pi_c^\dagger \rightarrow \pi_d \pi_d$ energy transfer channel as the dominant one, in our theory. Another annihilation mode in our theory would be a $\pi_c\pi_c^\dagger \rightarrow Z' \rightarrow \text{SM}$. The π_d decay into two Z' s is also an allowed channel, although with lesser contribution. The π_c and π_c^\dagger can annihilate to form the unstable diagonal π_d , which can further decay directly into SM particles, or through the intermediate Z' , as mentioned before.

We therefore have a few key parameters to work with: (a) The couplings between the dark pions; (b) couplings of Z' to SM and dark sector fermions (b) Mass of the DM fermions; (c) Mass of the bound state pions; (d) Mass of an additional vector particle Z' (which maybe constrained by LHC experiments). See figures [3.1](#) and [3.2](#)

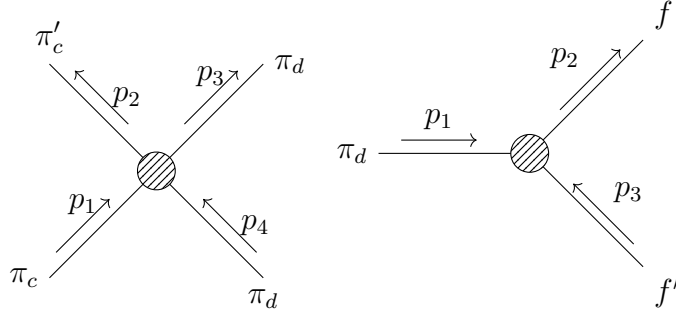


Figure 3.1: The main annihilation channels for DM to SM energy transfer via unstable dark pion to SM fermions

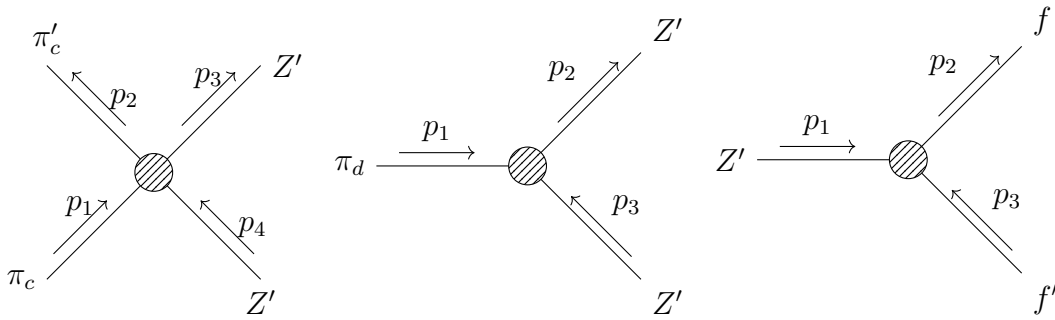


Figure 3.2: DM to SM decay via an additional Z' vector mediator which can decay into SM fermions

3.1.1 Simplified model implementation

Having described our model in detail, we implement our model in micrOmegas. We shifted tools from MadDM to **micrOmegas** [13, 14] which is an automatic DM observable calculator.

To start with, we ignore the presence of the Z' and simply look at the energy transfer via the unstable dark pion portal. For simplicity while calculating, we also approximate the confined bound states as scalars. Therefore, in these approximate calculations π_c and its conjugate represent a complex scalar particles, and the π_d represent a real scalar. Such an approximation works as we intend to use confined states which resemble SM pions which happen to be psuedo-scalars themselves (carrying a net spin of 0).

Lagrangian for the Simplified Model

$$L_{DM} \supset g_{DM} \pi_c \bar{\pi}_c \pi_d \pi_d + g'_{DM} \pi_c \bar{\pi}_c \pi_d - M_{\pi_d}^2 \pi_d \pi_d - \lambda_{\pi_d} \pi_d^4 \quad (3.1)$$

$$- M_{\pi_c}^2 \pi_c \bar{\pi}_c - \lambda_{\pi_c} (\pi_c \bar{\pi}_c)^2 + \sum_f g_f \bar{f} \cdot f \pi_d$$

Firstly, we would like to have an understanding of what would be the appropriate degrees of freedom depending on the temperature in the early universe. We therefore look at how the Freeze-out temperature varies with the mass of the DM candidate in figure 3.3.

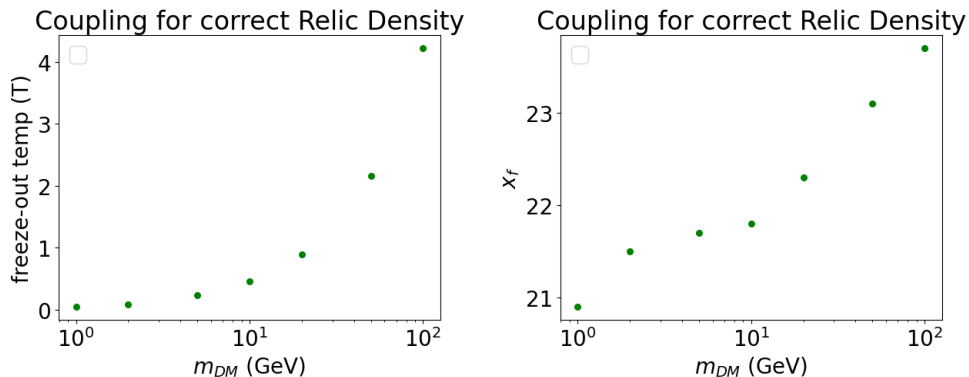


Figure 3.3: We show the Freeze-out temperatures for different DM mass candidates. Here, x_f and T are related as, $x_f = m/T$. T is measured in GeV.

We see, what value of couplings are needed to get the correct RD for certain masses of DM, and temperatures in the early universe [3.4](#).

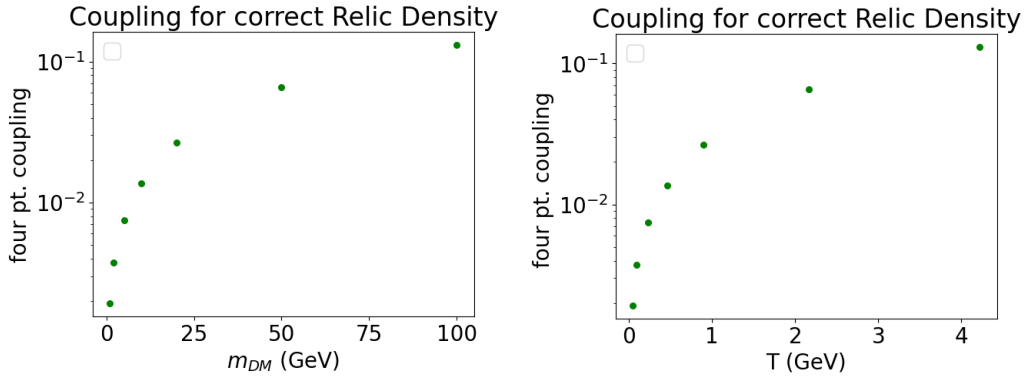


Figure 3.4: Here, x_f and T are related as, $x_f = m_{DM}/T$. We have plots for the coupling coefficients corresponding to the vertex between the π_d and π_c .

We can keep in mind that increasing the coupling strength of an energy transfer channel and the mass of the DM candidate reduces the eventual RD based on the reasons sighted before.

3.1.2 Effective Theory for the Dark Pion picture

Moving away from the toy model, we make two important additions to it. We not only need to add a Z' (some Z' theory can be seen in [\[15\]](#)) vector mediator, but also need to consider the appropriate Effective Field Theory for the energy scales with which we are dealing with.

As discussed, the picture of the DM model which we bring to light mimics a SM strong sector, driven with QCD like mathematics, with the exception of having only one generation of up and down dark quarks/fermions carrying *dark colour* indices. However, we work with a confined dark meson/pion like picture, because of temperature of the early universe at the time of DM freeze out. Hence we need to look closely at the construction and mathematics of a suitable effective field theory of this dark Pion model, which would best represent our case.

In the visible sector, we use the leading term of the *chiral Lagrangian* to explain the theory and write the Lagrangian for the confined picture. The chiral Lagrangian can be

reached by expanding the following expression which we receive from the Chiral perturbation theory,

We have, Σ

$$\Sigma = \exp 2i\Pi/f$$

$$L_0 = \frac{f^2}{4} \text{Tr} \delta\Sigma^\dagger \delta\Sigma = \text{Tr} \delta\Pi \delta\Pi + \frac{1}{3f^2} [\delta\Pi, \Pi]^2 \quad (3.2)$$

Here, Π is the field corresponding to the pions which we consider, f is the meson decay constant.

Instead of dealing with Gell-mann matrices as in the case of SM pions, we use a SU(2) structure. The meson matrix $\Pi \equiv \pi_a T_a$ (with $T_a = \Sigma_a^p = \sigma_i / \sqrt{2}$, the Pauli vector components) appears in the exponent of Σ is a traceless 2×2 matrix.

We therefore have,

$$\Pi_d = \frac{1}{\sqrt{2}} \begin{bmatrix} \pi_1^d & \pi_2^d - i\pi_3^d \\ \pi_2^d + i\pi_3^d & -\pi_1^d \end{bmatrix} \quad (3.3)$$

which, as we can understand has contribution from all three Pauli-matrices,

$\Pi_d \equiv \pi_a^d \cdot \Sigma_a^p$. In the dark pion matrix one can consider the diagonal components to be like π_0 from the SM pion theories, and the cross component to resemble the π_+ and π_i SM analogues. Therefore, we call $\pi_1^d = \pi_0$, $(\pi_2^d - i\pi_3^d) = \pi_+^d$ and $(\pi_2^d + i\pi_3^d) = \pi_-^d$

Substituting [3.3](#) in [3.2](#) we have the following expansion.

We look at the first term,

$$Tr[\delta\Pi_d\delta\Pi_d] = Tr\frac{1}{2} \begin{bmatrix} \delta\pi_0^d & \delta\pi_+^d \\ \delta\pi_-^d & -\delta\pi_0^d \end{bmatrix} \begin{bmatrix} \delta\pi_0^d & \delta\pi_+^d \\ \delta\pi_-^d & -\delta\pi_0^d \end{bmatrix} \quad (3.4)$$

$$Tr[\delta\Pi_d\delta\Pi_d] = \frac{1}{2} [(\delta\pi_0^d\delta\pi_0^d + \delta\pi_+^d\delta\pi_-^d) + (\delta\pi_-^d\delta\pi_+^d + \delta\pi_0^d\delta\pi_0^d)]$$

and for the second term,

$$\begin{aligned} & \frac{1}{3f^2} Tr[\delta\Pi_d, \Pi_d]^2 \\ &= \frac{1}{3f^2} Tr[\delta\Pi_d\Pi_d - \Pi_d\delta\Pi_d]^2 \\ &= \frac{1}{6f^2} Tr \left| \begin{bmatrix} \delta\pi_0^d & \delta\pi_+^d \\ \delta\pi_-^d & -\delta\pi_0^d \end{bmatrix} \begin{bmatrix} \pi_0^d & \pi_+^d \\ \pi_-^d & -\pi_0^d \end{bmatrix} - \begin{bmatrix} \pi_0^d & \pi_+^d \\ \pi_-^d & -\pi_0^d \end{bmatrix} \begin{bmatrix} \delta\pi_0^d & \delta\pi_+^d \\ \delta\pi_-^d & -\delta\pi_0^d \end{bmatrix} \right|^2 \\ &= \frac{1}{6f^2} Tr \left| \begin{bmatrix} (\delta\pi_0^d\pi_0^d + \delta\pi_+^d\pi_-^d - \pi_0^d\delta\pi_0^d - \pi_+^d\delta\pi_-^d) & (\delta\pi_0^d\pi_+^d - \delta\pi_+^d\pi_0^d - \pi_0^d\delta\pi_+^d - \pi_+^d\delta\pi_0^d) \\ (\delta\pi_-^d\pi_0^d - \delta\pi_0^d\pi_-^d - \pi_-^d\delta\pi_0^d - \pi_0^d\delta\pi_-^d) & (\delta\pi_-^d\pi_+^d + \delta\pi_0^d\pi_0^d - \pi_-^d\delta\pi_+^d - \pi_0^d\delta\pi_0^d) \end{bmatrix} \right|^2 \end{aligned}$$

Simplifying we get,

$$\begin{aligned} \frac{1}{3f^2} Tr[\delta\Pi_d, \Pi_d]^2 &= \frac{1}{6f^2} (\delta\pi_+^d\pi_-^d - \pi_+^d\delta\pi_-^d)^2 + 4(\delta\pi_0^d\pi_+^d - \pi_0^d\delta\pi_+^d)(\delta\pi_-^d\pi_0^d - \pi_-^d\delta\pi_0^d) \\ &\quad + (\delta\pi_-^d\pi_+^d - \pi_-^d\delta\pi_+^d)^2 + 4(\delta\pi_-^d\pi_0^d - \pi_-^d\delta\pi_0^d)(\delta\pi_0^d\pi_0^d - \pi_0^d\delta\pi_+^d) \end{aligned}$$

Upon further simplification and combining similar terms the Lagrangian looks like,

$$\begin{aligned} L &= \delta\pi_0^d\delta\pi_0^d + \delta\pi_+^d\delta\pi_-^d + \frac{1}{6f^2} [(\delta\pi_+^d\pi_-^d\delta\pi_+^d\pi_-^d) + (\delta\pi_-^d\pi_+^d\delta\pi_-^d\pi_+^d) - 2\pi_+^d\delta\pi_-^d\pi_-^d\delta\pi_+^d] \quad (3.5) \\ &\quad + \frac{2}{3f^2} [\pi_+^d\delta\pi_-^d\pi_0^d\delta\pi_0^d + \pi_-^d\delta\pi_+^d\pi_0^d\delta\pi_0^d - \pi_+^d\pi_-^d\delta\pi_0^d\delta\pi_0^d - \delta\pi_+^d\delta\pi_-^d\pi_0^d\pi_0^d] \end{aligned}$$

With the first two terms being the Kinetic terms for $\pi_{(+,-,0)}$ and the third term being the interaction terms for the dark pion vertex. In the model, we fix $m_{\pi_c} > m_{\pi_d}$. We stick to a default relation of $m_{\pi_d} = 0.9m_{\pi_c}$, but also study what happens upon varying this mass difference.

We once again start with documenting how the Freeze-out temperature depends on the mass of the DM candidate in figure 3.5. Note that the following results do not include the presence of the Z' channel. The data closely resembles the toy model. This allows us to understand what phase of the DM candidates we need to consider, for our Freeze-out calculations. As we can see, the typical DM Freeze-out temperatures, lie around 4-5 GeV, which is much lesser than the pion DM masses which we consider. This would therefore mean that the temperature around the DM Freeze-out point is not high enough to break them into their component Dirac DM form, and allows us to work with the pion DM phase only, safely assuming that the DM will be in the confined state.

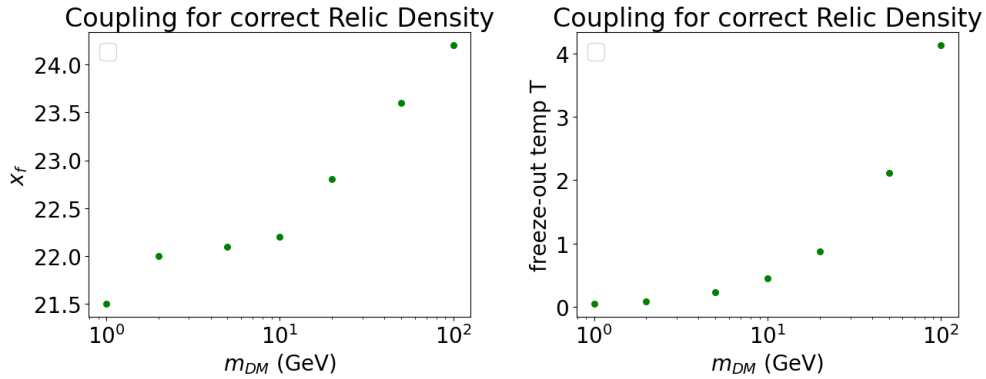


Figure 3.5: Here, x_f and T are related as, $x_f = m_{DM}/T$. The data closely resembles the toy model. The x-axis in both the plots are log-scaled.

We then look at how the coupling terms of the π_c - π_d vertex affect the RD behaviour along with the DM candidate masses. Notably, we observe a major difference when we look at the values of the couplings needed to get the correct RD as compared to the toy model in the behaviour in figures 3.6. We have a decreasing trend as compared to the previous increasing trend. This can be explained, using the likes of equation 2.23. The momenta dependent vertex implies an increase in the energy transfer to the SM sector with the increasing momenta. A higher candidate mass also leads to a higher value of this integral leading a reduced RD. Therefore, in-order to get the correct RD we need to compensate in the coupling value (lower coupling values).

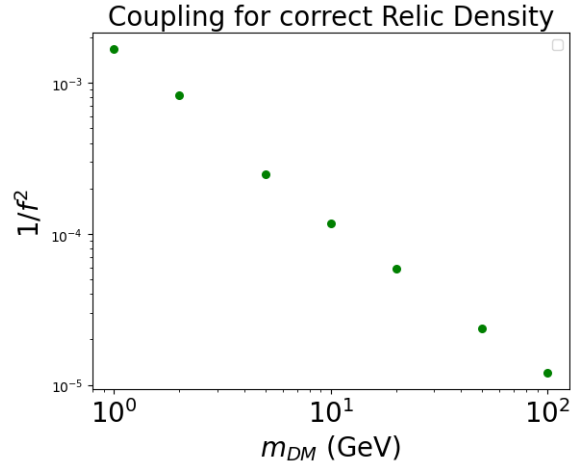


Figure 3.6: A plot showing the coupling (which has been written in terms of the pion decay factor f) required to give the observed value of RD for different masses of DM.

We look at the same calculation, but instead with the term f alone on the y-axis as in the dark-pion Lagrangian [3.7](#).

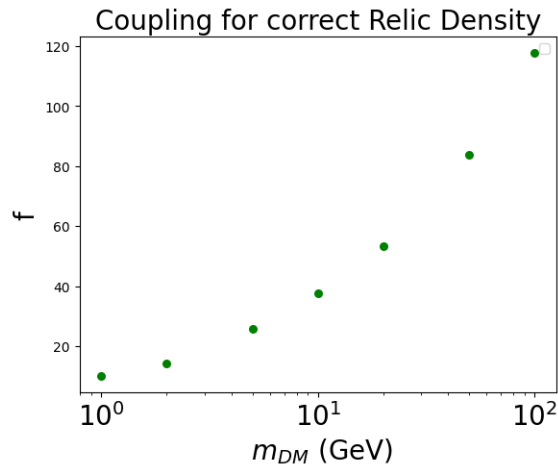


Figure 3.7: A plot showing the value of f required to give the observed value of RD for different values of DM masses.

Finally, we also recall that we have been using a 10% mass difference between the stable and unstable dark pions for all our calculations. We look at figure [3.1.2](#) to see what f values we require to get the correct value of the RD for varying differences between the diagonal and cross pions across a mass range. Predictably we see that, an increase in mass (with cross (stable) pion having a greater mass than diagonal (unstable) pion) difference, increases the value of the required f , since increasing the difference between the DM particles and the mediator increases the reaction rate and thus demands a lesser value of coupling strength of the vertex.

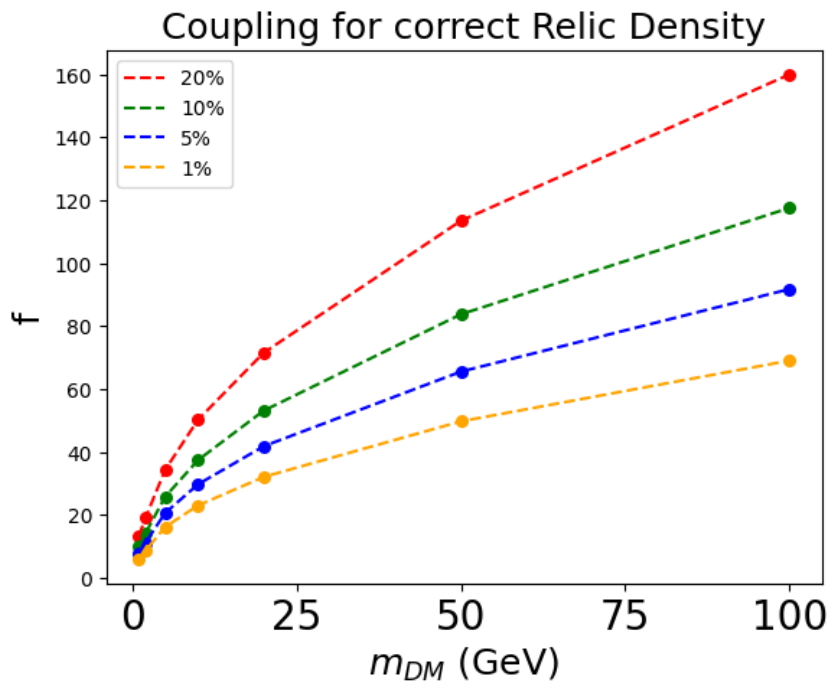


Figure 3.8: A plot showing the value of f required to get the correct RD for values of m_{DM} ranging from 1-100 GeV and each with four different cases of percentage difference between masses of π_c and π_d .

3.2 Adding a $U(1)'$ charged vector boson Z'

We now look at how our results change upon adding the vector mediator Z' which can be a mediator between SM and DM sectors.

While dealing with pseudo-scalars like the dark pions in our case, we need to consider their axial currents. For the process, $\pi_{DM}\pi_{DM} \rightarrow Z'$, after which the Z' decays into SM fermions, we note that we are looking at two pseudo scalar spin-1 particles annihilating with each other to give rise to a spin 1 vector mediator. Clearly, in-order to conserve the spin, we can only use the spin-0 component of the vector mediator, i.e. the longitudinal component of the vector mediator. It has been shown that decay of pions can only happen through axial vector component corresponding to the current.

$$j_5^\mu = \bar{\psi}\gamma^\mu\gamma^5\psi$$

The axial (chiral) current is the Noether current for the axial transformation,

$$\psi(x) \rightarrow e^{i\alpha\gamma^5}\psi(x)$$

with $\alpha \in R$ denoting a continuous symmetry.

A thorough examination of the new physics encountered upon introducing the heavy Z' mediator alongside the already existing strong channel revealed many interesting features of our theory and made it colorful (just the adjective) in many ways. As we will soon find out, there are three channels for energy transfer, depending upon the parameters at use. The strong channel (SC), as we have already discussed, is the case where the energy transfer takes place completely or dominantly via the unstable dark pions and the subsequent decay mechanisms. Two more channels which came into light upon the introduction the heavy boson, a Z' pair channel (ZC), and a Z' resonant channel (RC). The interplay of energy transfer through the two mediators is what will be looked at in the next section.

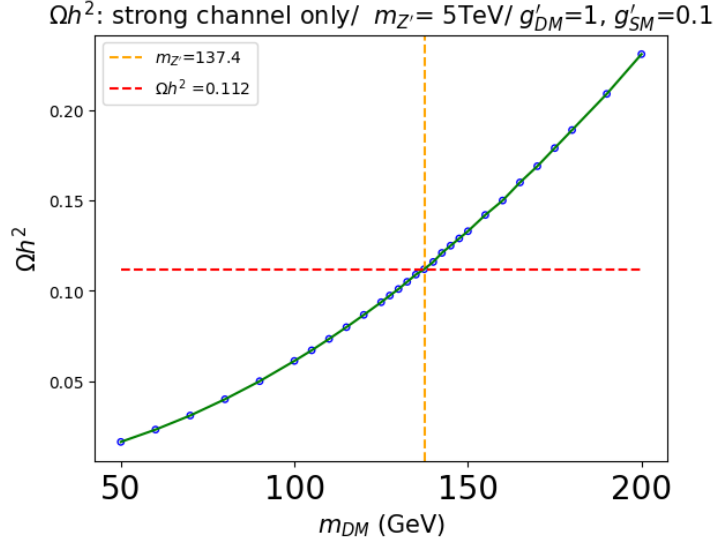


Figure 3.9: We show the point of intersection between the $\Omega h^2 = 0.112$ line and the curve which shows how the RD changes with the mass of the DM.

3.2.1 The strong annihilation channel

For the limiting case that Z' is quite a heavy particle as compared to our dark matter candidate (taken to be in the 1-1000 GeV mass range), we once again shall almost entirely have the SC case as we had showed before, but with a slight modification. The pion decay factor f has experimentally studied to be proportional to the mass of the dark pion. Hence for further calculations we have fixed $m_{DM} = f$ to have one lesser parameter to deal with. Although this keeps the new strong sector qualitatively identical to the previously discussed behaviour, it changes quantitatively. For instance, the new $m_{DM} = f$ value for which the SC gives the correct RD is 137.4 GeV instead of the previous $f = 117.6$ GeV at $m_{DM} = 100$. Referring to figure [3.9](#), here g'_{DM} and g'_{SM} are the couplings of the Z' to DM and SM respectively (although it doesn't matter in this plot, it does play a role in subsequent ones where ZC is important). Here the mass of the Z' particle is fixed at 5 TeV.

3.2.2 Interplay between the Z' channel and strong channel

We now look at the case where Z' is light enough to allow annihilation via $\pi_c \pi_c^\dagger \rightarrow Z' Z'$. Such low masses may be allowed if coupling to SM is small but DM is large. We return to

this at the Z' channel (ZC).

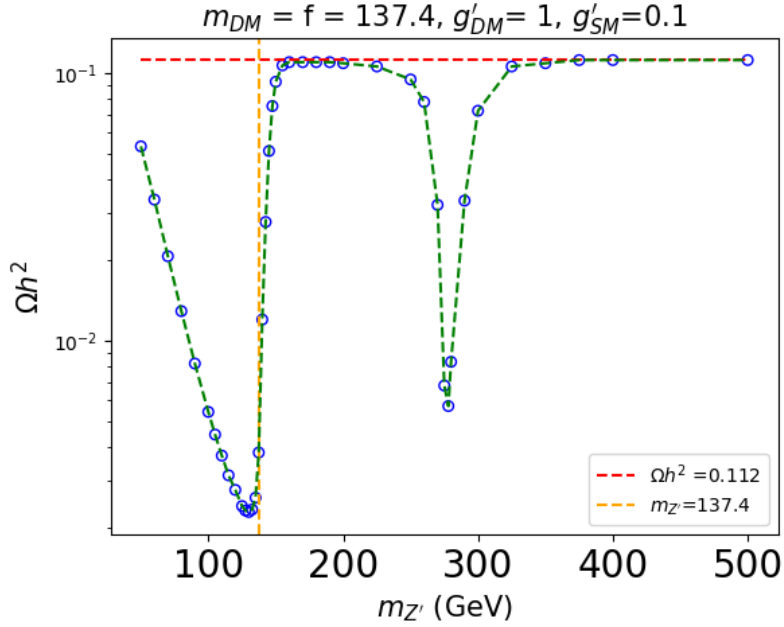


Figure 3.10: Change in RD with DM mass for the ZC. All the parameter values are displayed in the plots. With exception that the second plot shows a scaled x axis as shown, the two plots are identical.

Firstly we see the complete interplay between ZC and SC with varying of the mass of Z' ($m_{Z'}$), keeping f and m_{DM} at a fixed value in figure [3.10](#). Starting with $f = m_{DM} = 137.4$ GeV (which gives us the correct RD), the $\pi_c \pi_c^\dagger \rightarrow Z' Z'$ channel is open for $m_{Z'} \leq f$ (close to each other). As the $m_{Z'}$ decreases from 137.4 GeV to 50 GeV we go away from $m_{DM} = m_{Z'}$ and the ZC channel contribution decreases, hence increasing the RD. The increase of RD is steeper for $m_{Z'} > m_{DM}$ since the contribution of the ZC falls off quicker (due to kinematic conditions). After a sufficiently large value of $m_{Z'}$ as compared to m_{DM} , the SC which is always active due to the comparable masses of the stable and unstable dark pions, is the only contributing channel and the RD settles onto the RD = 0.112 as shown. However when $m_{Z'}$ is around 2 times the mass of the DM we hit the resonant channel (RC) for the DM $DM \rightarrow Z'$ annihilation and we see a steep fall in RD around this region. We shall study this in the next section

In the same spirit, we also look at how changing the coupling between the vector particle and DM, g'_{DM} affects the same results in figure [3.11](#).

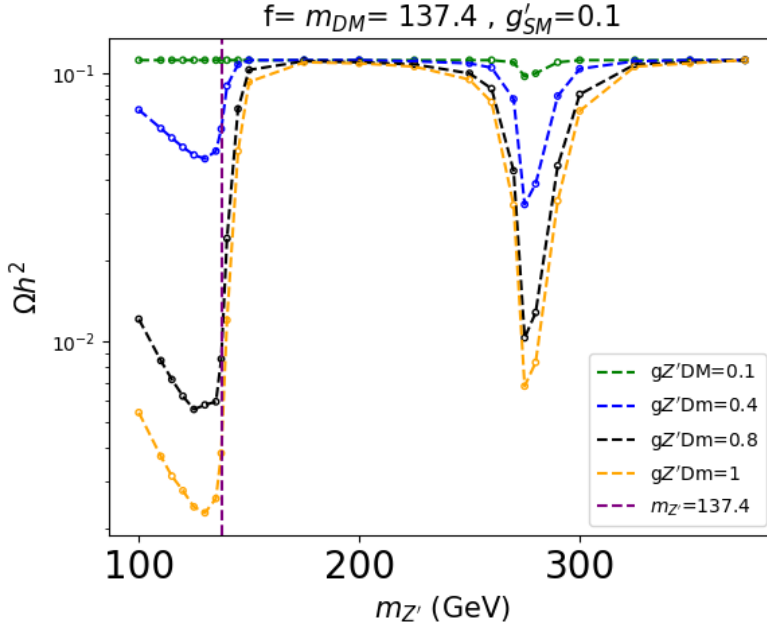


Figure 3.11: Quite clearly, as we decreased g'_{DM} from 1 to 0.1, the strength of the coupling and the rate of the annihilation reaction decreased, thereby increasing the value of RD as a general trend.

With clarity about the general interplay of the two channels and the behaviours, we must also look at how varying f (and m_{DM}) and $m_{Z'}$ simultaneously, keeping the couplings fixed affect the RD in figures 3.12 and 3.13. We have both line plots and contour plots to explain the same.

In figure 3.12 we see how the behaviour of the RD curves changes with value of f . As expected they resemble figure 3.10, with the $m_{Z'}$ values of the two minimas in RD shifted depending on the value of f used. The same thing can be seen in the contour plot in figure 3.13 upon close inspection. The contour plot is more useful to distinguish the 0.11 contour and hence distinguish the acceptable region in our parameter space. We have scanned across relatively small region of parameters here (with the discreteness arising due to a step size of 25 GeV for our data points). We also see a subsequent percentage contribution plot of the SC for the same sets of parameters instead of RD. Clearly, the curves have quite a similar appearance when it comes to the positions of the minimas. Since the SC is always turned on, a drop in contribution of SC would mean the switching on of the ZC and RC (depending on the position of the minimas respectively). This would mean higher cross-section in the region and hence lower value of RD.

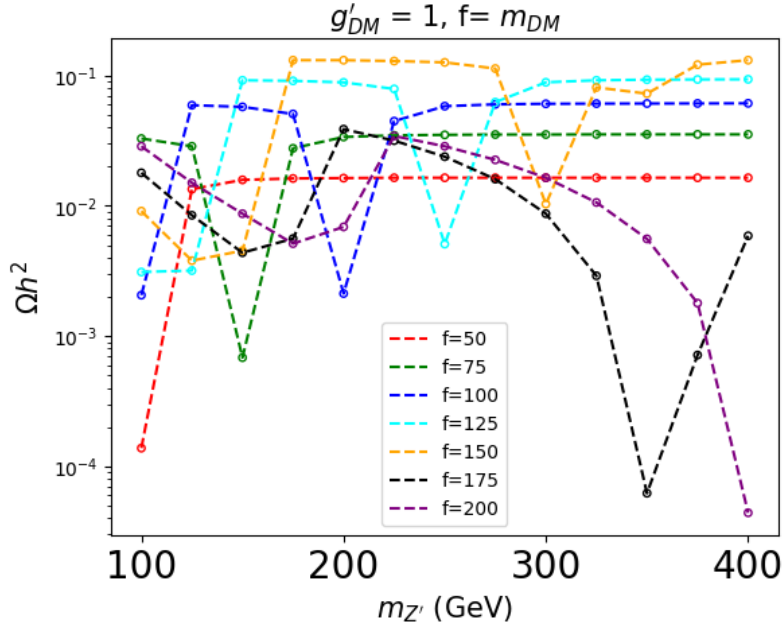


Figure 3.12: RD values while scanning $m_{Z'}$ from 50 GeV - 400 GeV and m_{DM} scanned from 25 GeV - 250 GeV.

The same exercise is also performed on a wider range of $m_{Z'}$ and f values which makes it much useful for our purposes. We can notice in figure [3.14](#), the two regions (/lines if we had a more continuous set of points) of minimas, one of them around $m_{Z'} = f$ (both SC and ZC active) and the other one around $m_{Z'} = 2f$, as is consistent with our previous observations. This potentially allows four different values of $m_{Z'}$ for each value of f which can give us the correct RD value. Given that each minimum is surrounded by the 0.1 contour as can be seen, we can clearly understand how a $f = 400$ GeV (say) line cuts the 0.1 contour at four different locations (roughly speaking, around 100, 400, 700 and 900 GeV). For instance we can also gauge that, given our choice of not considering DM masses in excess of 1 TeV, we need not consider $m_{Z'}$ in excess of 2.1 TeV. Note that the islands of minima can actually be considered to be a connected, linear region. The output is simply a manifestation of the granularity of the parameters scanned.

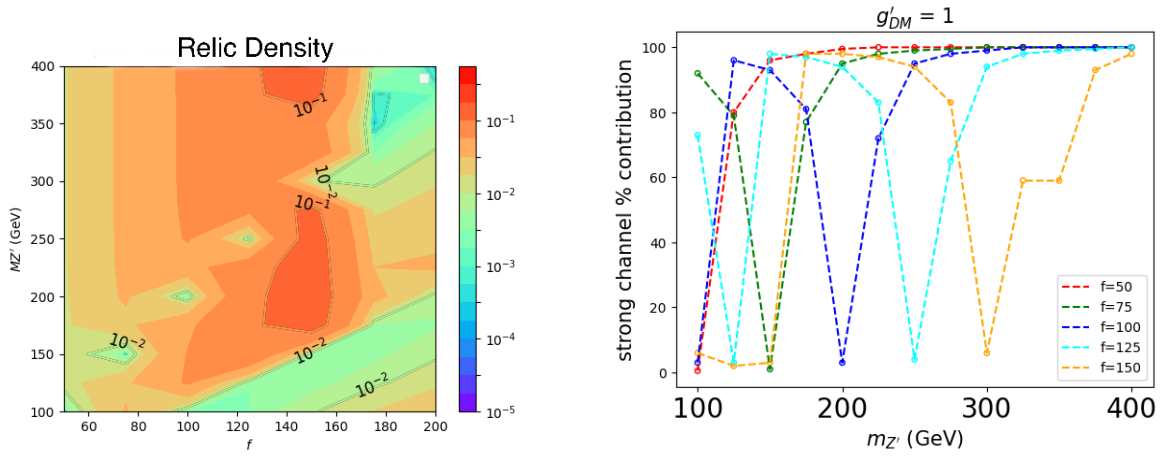


Figure 3.13: The image on the left provides the contour plot for mapping the RD across the two parameters f and $m_{Z'}$ for figure 3.12. The image on the right shows the percentage contribution from the strong channel for the same sets of parameters.

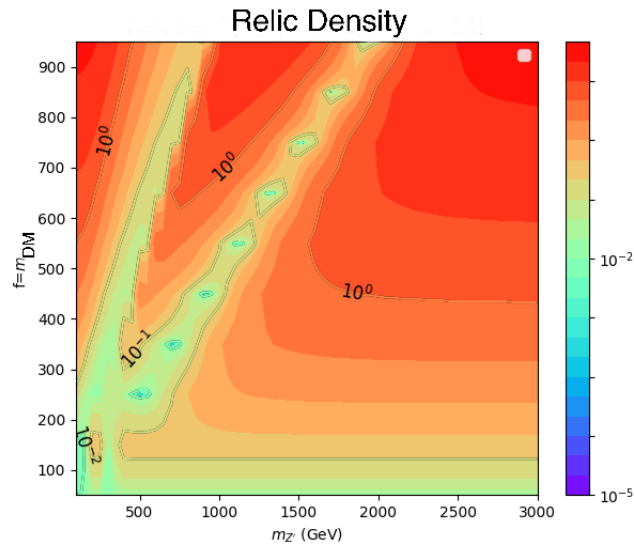


Figure 3.14: The contour plot for mapping the RD whilst varying the parameters f and $m_{Z'}$ across the larger ranges, $f = 50 - 1000$ and $m_{Z'} = 100 - 3000$ GeV.

3.2.3 The Z' Resonant channel

Having studied the interplay between SC and ZC we now shift our attention to the Resonant channel (RC). We now have three parameters fixed instead of two $m_{DM} = f = m_{Z'}/2$. We thereby vary m_{DM} and see the behaviour of the RD as in figure 3.15. As we are dealing with the resonance condition, we now have the curve cutting the RD= 0.112 line at much higher values, due to the higher annihilation rates corresponding to the RC. At higher masses, the cross-section of interaction to decay via the DMDM $\rightarrow Z' \rightarrow f\bar{f}$ process is lower, and hence the higher RDs. The sharp dip starting from $m_{DM} \approx 160$ - 165 GeV can be explained by opening of a new channel, DMDM $\rightarrow Z' \rightarrow t\bar{t}$ (the mass of the top quark around a 172 GeV which favours the decay of Z' into the top quark and anti-quark).

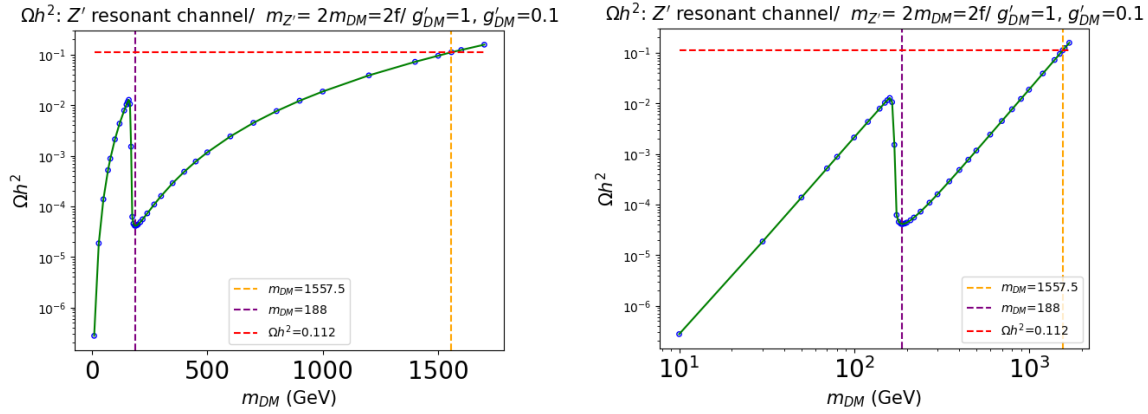


Figure 3.15: We vary $m_{DM} = f = m_{Z'}/2$ and look at the behaviour of RD once again. We have marked two points on the curve using the $x = 1557.5$ and $x = 188$ lines. We have two variations of the same plot, the first one being a log-linear plot, and the second one being a log-log plot.

3.2.4 Dependence of RD on pion mass difference

For completeness we also look at how the difference between masses of the stable and unstable dark pion affect the RD. We change the difference in masses from 1% to 20% in figure 3.16. Clearly, the larger the mass difference between the two dark pions (with unstable pion having the lower mass), the easier it is for two stable dark pions to annihilate into two unstable dark pions and hence, the channel shall have the higher cross-section, thereby reducing the RD. For the following plots, the values of m_{π_c} where each curve corresponding to a certain

value of $\delta m/m_{\pi_c}$ (in percentages) intersect the $RD = 0.112$ line are, 50 GeV, 85 GeV, 137 GeV, 192 GeV, 250 GeV and 560 GeV for percentage differences of 1, 5, 10, 15, 20, and 50 respectively.

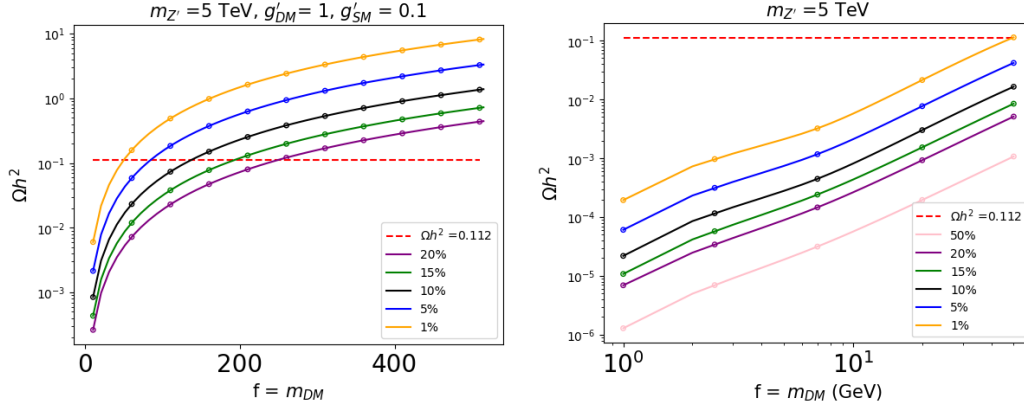


Figure 3.16: We vary m_{π_c} and look at the percentage difference between masses of the stable and unstable dark pion for the SC by setting $m_{Z'} = 5\text{TeV}$. We also have the same plot for a narrower and log-log scaled mass range where we encounter a linear increase.

We also have a contour plot for the same where we can simply look at the 0.1 contour for simplicity in figure [3.17](#).

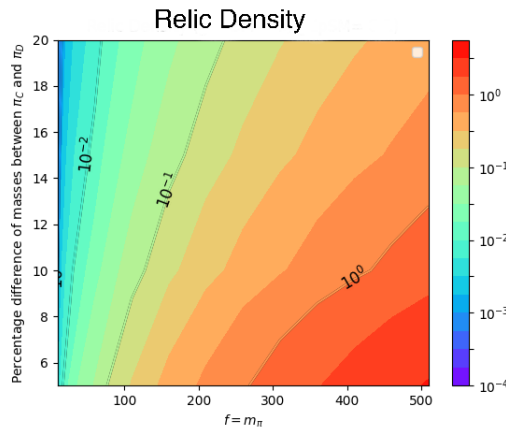


Figure 3.17: A contour plot showing the RD for varying the percentage difference between the DM candidate and the diagonal Pion mediator (in percentage) of the SC and the value of f and m_{DM} .

Chapter 4

Complementary Signatures of SIDM

In this chapter, we look at detection prospects of our model via direct or indirect detection searches.

4.1 Direct Detection of Dark Matter

We look at the interaction of DM particles with fixed nucleon targets, by their collision with the nucleons. In this regard, we are essentially interested in a t-channel interaction between the DM particle (or anti-particle) and the nucleons used in the experiment, or more specifically, the up and down quarks (or anti-quarks) which constitute the nucleons.

The interaction between the DM pions and SM particles happen only through the Z' and only via the longitudinal component. This is proportional to the axial vector current component of the interaction between Z' and SM fermions due to the involvement of a pseudoscalar spin 0 DM, and the need to have the spins aligned for the interactions to be enabled. This resulted in us using the axial vector component of the vector current involved only, which also has spin 0. Given how the relevant part of the Lagrangian therefore looks,

$$L_{DM} \supset g'_{SM} \sum_f m_f (\bar{f} \gamma^\mu \gamma^5 f) Z'_\mu \quad (4.1)$$

$$L_{DM} \supset g'_{SM} \sum_f m_f (\bar{f}_L \gamma^\mu \gamma^5 f_R + \bar{f}_R \gamma^\mu \gamma^5 f_L) Z'_\mu \quad (4.2)$$

We understand that there is a fermion mass proportionality factor in the above terms. This therefore makes the interaction between our DM candidate and the lightest quarks, up and down extremely weak, as a result of which we do not see an interaction between DM and nucleons of the target.

In the case of our model, we find the scattering cross-section between the dark pion (cross) in our theory and nucleons to be zero, i.e. there exists no interaction between the Hadrons used in colliders for the scattering experiments and the DM candidate. This leads to zero exclusion constraints set by Direct detection. Since there exists no interaction of our DM theory with a rather stringent constrain-er of most DM theories, we have essentially found a way to by-pass an important filter and have the license of using a large part of our parameter space.

4.2 Indirect Detection of Dark Matter

We already provided a brief introduction of Indirect detection of DM in the section [1.3](#). Here we look at the theory of Indirect detection [16](#) a bit more closely, followed by the results from our model.

As mentioned before, should primordial self-annihilations take place in the early universe, the same process would take place now in the denser regions of the galactic DM halo, which correspond to higher densities of DM. At the core of such galaxies, the high temperatures can re-activate processes such as the different DM annihilation channels active in the early universe (with the availability of higher energies) which had frozen as the universe expanded. DM annihilation in the Galactic halo produces pairs of Standard Model particles that hadronize and decay into stable particles. The final states with γ , positrons, anti-protons, and neutrinos are particularly interesting and they are the subject of indirect searches. In general the production rate of particles from DM annihilation at location x has a form,

$$Q_a(\mathbf{x}, E) = \frac{1}{2} \langle \sigma v \rangle \frac{\langle \rho(\mathbf{x})^2 \rangle}{M_{DM}^2} f_a(E) \quad (4.3)$$

where, $\rho(\mathbf{x})$ is the DM mass density at the location \mathbf{x} and $f_a(E) = \frac{dN_a}{dE}$ is the energy distribution of the particle a produced in one reaction. $\langle \sigma v \rangle$ is the annihilation cross-section times the relative velocity of incoming DM particles which we evaluate in the limit $v = 0$.

4.2.1 Annihilation channels and fluxes observed

We consider DM annihilation (parameterized by the DM DM cross section $\langle \sigma v \rangle$) and decays (described by the DM decay rate $\Gamma = 1/\tau$) into the following primary channels:

$e_L^+ e_L^-, e_R^+ e_R^-, \mu_L^+ \mu_L^-, \mu_R^+ \mu_R^-, \tau_L^+ \tau_L^-, \tau_R^+ \tau_R^-, \bar{q}q, \gamma\gamma, gg$, decays into the three types of neutrinos and their anti-neutrinos, or finally, decay into two vector mediators which give decays into 4 leptons. Here, q refers to the quarks, g refers to gluons and h refers to the higgs particle.

The particles produced in Dark Matter annihilation/decay will be provided with parton showers and hadronization, in such a way to eventually obtain the fluxes of, $e^\pm, \bar{p}, \bar{d}, \gamma, \nu^{e,\mu,\tau}$ and $\bar{\nu}^{e,\mu,\tau}$, where, the study of their excess is the most commonly used for characteristic indirect detection studies of DM.

4.2.2 Using Pythia

Since we have non-standard decay modes, we cannot use the basic pure modes that are hard-coded in micromegas. We therefore use Pythia to obtain the exact spectrum of the four commonly studied fluxes. PYTHIA is a program for the generation of high-energy physics collision events. For more information on installation and general details one can refer to [17], or visit [Pythia](#). Pythia's algorithm provides us with the respective energy fluxes which we can then use to compare with real data as in [18, 19, 20]

We present the data for the fluxes of photon, anti-proton, positron and neutrinos, as predicted by our model in the following sections. As mentioned, the computations were performed via Pythia. These energy spectra, are expected to be present in addition to the

usual observed background fluxes from other SM processes (which is typically modelled as approximately $\frac{d\phi}{dE} \propto E^{-2}$). We present figures showing the number density per energy bin $\frac{dN}{dE}$, for each of the fluxes, across the energy spectra $0 \rightarrow 250$ GeV, for two cases of DM masses each with the cases of Z' resonance and the strong channel. We note that, all of the measurements have been made taking, the coupling values, $g'_{DM} = 1$ and $g'_{SM} = 0.1$.

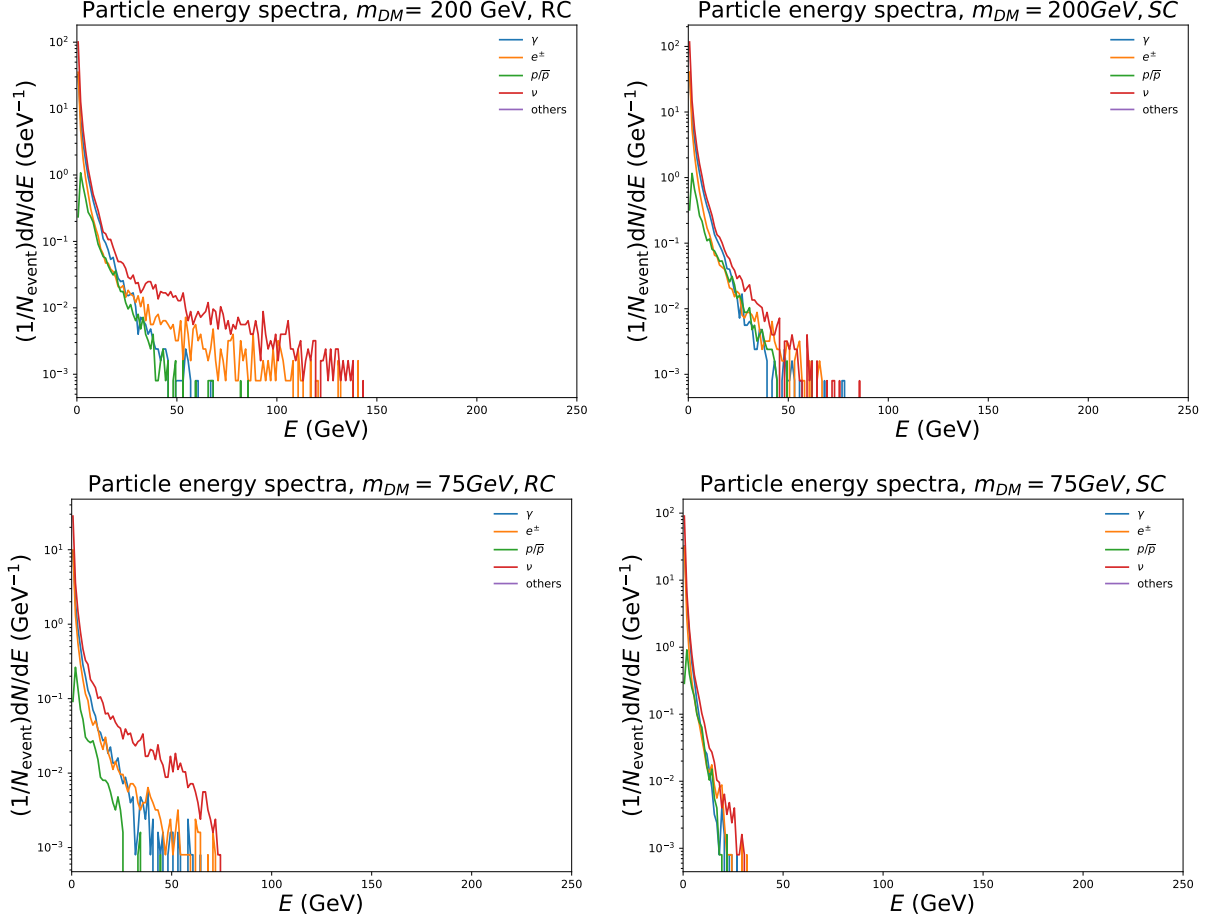


Figure 4.1: We show the four kinds of fluxes, for four different cases in the parameter space. Here, RC denotes the Z' resonant channel and SC denotes the strong channel.

A characteristic feature of both the cases which we observe is that in the case of the Z' resonance, we see our final state products accessing higher energy bins, and hence the fluxes are more spread out across the energy range than the case including the strong channel only. This is a direct consequence of the fact that the presence of a case allowing a heavy mediator, brings additional mass-energy to the table, whose decay products, as a consequence can also access higher energies.

4.2.3 Prospects for Indirect Detection

We compare the photon energy spectra as simulated by Pythia and predicted by our model to observations of Cherenkov Telescope Array (CTA). We present a comparative figure showing the upper limit (95% containment limit (C.L.) ; sensitivity plot) for the observed background photon energy spectra observed by CTA, to our signal simulation. If the signal (spectra due to the DM candidate), is not contained within this upper limit, it would mean that we could potentially observe annihilation events giving the energy spectra via CTA. If not, then even though our model isn't ruled out, there would be no way of confirming our hypothesis by distinguishing such signals from the background uncertainties (see figure 6 [18]).

We used the following general expression (for mass-less particles) for going from number of photons per energy bin per annihilation, to the differential flux observed per energy bin, for photon fluxes, so that we can compare our simulation with the available data.

$$\frac{d\Phi_\gamma}{d\Omega dE_\gamma}(E_\gamma, \psi) = \frac{1}{4\pi} \int_{l.o.s.} dl(\psi) \rho_{DM}^2(r) \left(\frac{\langle\sigma v\rangle_{ann}}{2S_{DM}m_{DM}^2} \frac{dN_\gamma}{dE_\gamma} \right) \quad (4.4)$$

where the integration is performed along the line of sight (l.o.s.) in the observing direction (ψ). Here, $\langle\sigma v\rangle_{ann}$ is the average velocity-weighted annihilation cross-section, S_{DM} is a symmetry factor that is = 1 if the DM particle is its own anti particle and = 2 if not, N_γ is the number of photons per annihilation.

We used the value $7.1 \cdot 10^{22} \text{ GeV}^2 \text{ cm}^{-5}$ for the integral (taking the constants outside the integral from equation 4.4 we are left with the following expression, also called the J factor), corresponding to the one used in the calculations for CTA. The quantity is calculated based on the assumed DM distribution models in the galaxy (refer to section 5.3 in [18]).

$$J \equiv \int_{d\Omega} \Omega \int dl(\psi) \rho_{DM}^2(r) \quad (4.5)$$

Referring to figure 4.2, we see that the C.L. of the background spectra from CTA can be compared with the following two special cases encountered earlier. (a) $f = m_{DM} = 137 \text{ GeV}$, $m_{Z'} = 5 \text{ TeV}$, which represented the case which gave us the correct RD with the dominant mode of annihilation being the SC; (b) $f = m_{DM} = 1557.5 \text{ GeV}$, $m_{Z'} = 3115 \text{ TeV}$, which

represented the case which gave us the correct RD with the dominant mode of annihilation being the ZC. All other cases are an interplay between these two cases. Here, we had the coupling value of $g'_{DM} = 1$ and $g'_{SM} = 0.1$.

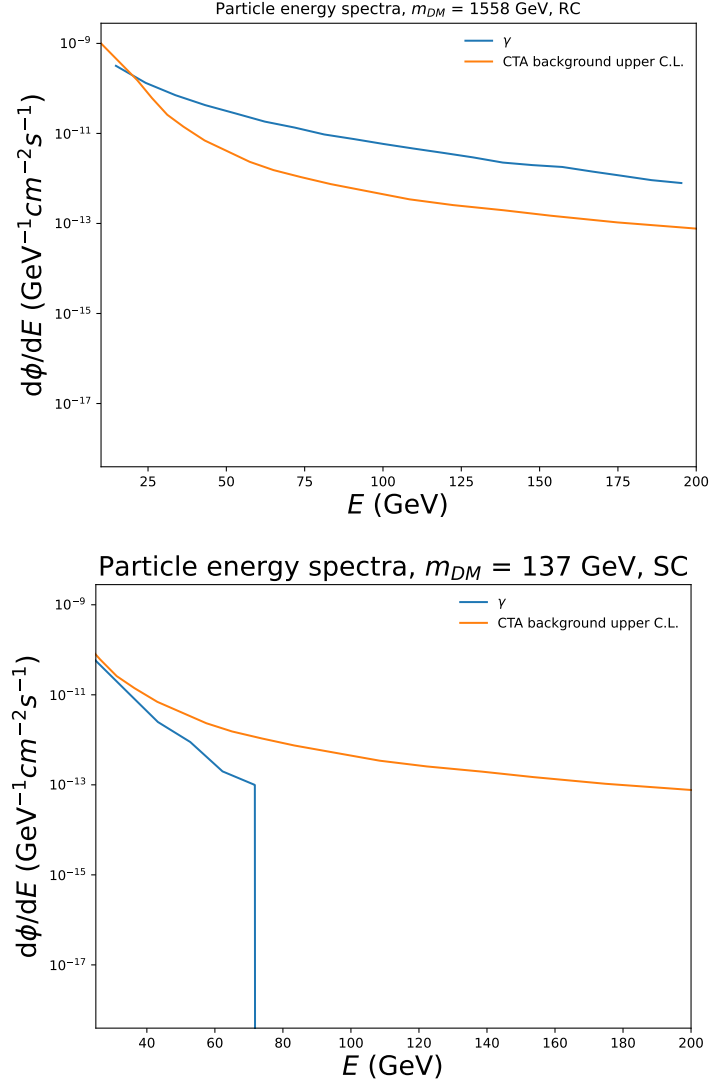


Figure 4.2: The simulated photon fluxes for the two cases, SC and ZC.

For the SC case in figure 4.2, the simulated fluxes does not exceed the C.L. However we see that for the RC case in figure 4.2, we see that the simulated energy fluxes exceeds the background C.L. implying that the model and the photon fluxes corresponding to its annihilation channels should be visible in CTA observations, for the used set of parameters. This suggests that the model should be verifiable through complementary signatures from Indirect detection, for some regions of the parameter space.

Chapter 5

Conclusion

In this work, we started off by studying, analyzing and reviewing the work presented in [4]. This allowed us to understand how a general DM model is built, and familiarized us with the relevant theories present behind this construction. We worked out various theoretical expressions and the scattering cross-sections of the different energy transfer channels in the theory, which get substituted into the Boltzmann equation, and in turn is used to calculate one of the most important restrictions of any DM theory, the Relic Density. We looked at how the parameter space affects the RD of any theory.

We then learnt to use multiple programs/tools such as MadDM, micrOmegas and Pythia, for the computation of DM observables, and put them to test to produce parameter spaces for different quantities of a few simple DM models already present in literature. We performed an in-depth analysis for the results of models with the motivation to carry out the same exercise for new and uncharted territories.

We worked on the construction of a novel, Strongly Interacting Dark Matter (SIDM) model. The model depicted a DM candidate which mimics a standard model stable pion, something which we call a dark Pion, which can decay into the visible sector via either an unstable dark pion (which will also be predicted to be present by the model which we constructed) or an additional heavy vector mediator which satisfies the required properties of such a model. Therefore, we also introduced an additional gauge group, $SU(3)'$ and the required indices, along with the particles, to make the theory complete. We analyzed the resulting parameter space, which comes to the forefront as a result of the phenomenolog-

ical description of the model, to look for an acceptable RD of DM, given by cosmological constraints. We looked at the results obtained from the two channels in details, and what interesting implications they present.

We also looked at complementary signals for the model simulated the energy spectra of the fluxes which we expect to observe via Indirect detection of the model, which can be compared to real life data. We verified through simulation that, the photon fluxes predicted by our model should be detectable over the background energy spectra of our galactic core, if such a model exists. We also reasoned as to why such a theory shouldn't be detectable using our current Direct detection experiments.

Appendices

Appendix A

A.1 Calculation techniques for Scattering Amplitudes and Cross-section matrices

We learn how the scattering amplitudes and cross-sections, which go into the useful Boltzmann equation solving codes for calculation of DM RD is calculated are constructed by calculating the same, present in the reference, [4] which we want to study. First, we start by calculating the scattering cross-section in the first figure of [2.7]. Here energy is transferred to the HS by annihilation of SM fermions to dark fermions via ohotons (or dark photons).

The scattering amplitude term for a s channel $f^+ f^- \rightarrow e^- e^+$ is given by,

$$\bar{v}^{s'}(p') \left(\frac{-iK_i \sqrt{4\pi\alpha} \gamma^\mu \cos\theta_\epsilon}{\cos\theta_W \sqrt{1-\epsilon^2}} \right) u^s(p) (-ig_{\mu\nu}/q^2) \bar{u}_{DM}^r(k) (-i\sqrt{4\pi\alpha'} \frac{\epsilon \cos\theta_\epsilon}{\sqrt{1-\epsilon^2}} \gamma^\mu) v_{DM}^{r'}(k') \quad (\text{A.1})$$

Here α' is the coupling constant for the dark fermions, α , the coupling constant for the usual electroweak interaction, the central term refers to the photon mediator, it's momentum q , and a $g_{\mu\nu}$ for index contraction. K_i is a constant which scales the value of the electric charge according to the fermion used

The above is a very simplified scattering amplitude based on the kind of DM Lagrangian that we are interested in. It ignores the Z Boson mediator term, the dark sector interaction, and the Z Boson decaying into two DM fermions at high enough energies as in the 3 Feynman diagrams displayed before. $|iM|$ can be written as,

$$\left(\frac{iK_i 4\pi \sqrt{\alpha\alpha'} \epsilon \cos^2 \theta_\epsilon}{q^2 \cos \theta_W (1 - \epsilon^2)} \right) (\bar{v}(p') \gamma^\mu u(p)) (\bar{u}_{DM}(k) \gamma_\mu \bar{v}_{DM}(k')) \quad (\text{A.2})$$

Here, if the u 's denote particle wave functions, the v 's with the same momentum label alphabet denote the corresponding antiparticle wave function. The primes associated with the momenta labels to differentiate the two particle momenta on either side of the vector gauge. \bar{x} denotes complex conjugates. Note that both u and v are defined by contraction of the particle field with the momentum eigenstate. Following on from this, $|M|^2$, $(iM(-iM^*))$ looks like,

$$\left(\frac{K_i 4\pi \sqrt{\alpha\alpha'} \epsilon \cos^2 \theta_\epsilon}{q^2 \cos \theta_W (1 - \epsilon^2)} \right)^2 (\bar{v}(p') \gamma^\mu u(p) \bar{u}(p) \gamma^\nu v(p')) (\bar{u}_{DM}(k) \gamma_\mu v_{DM}(k)' \bar{v}_{DM}(k)' \gamma_\nu u_{DM}(k)) \quad (\text{A.3})$$

Using the knowledge that we send fermions polarised in spin up or down state, for both of which we can construct a wave function owing to a certain momentum state, for the scattering experiment, we divide both sides by $(1/2)(1/2)$ and sum over all the spin state wave functions.

Finally, using the completeness relations we can write,

$$\sum_s u^s(p) \bar{u}^s(p) = \gamma^\mu p_\mu + m \quad (\text{A.4})$$

and for the anti-particles,

$$\sum_s v^s(p) \bar{v}^s(p) = \gamma^\nu p_\nu - m \quad (\text{A.5})$$

Note that we must think m as m multiplied by some identity operator, so that the LHS and RHS gives us a matrix equation.

Contracting all the indices in equation [A.3](#) and looking at the final result,

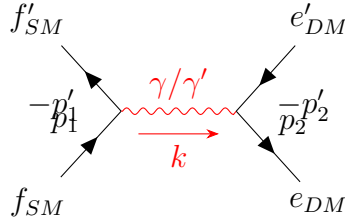
$$\left(\frac{K_i 4\pi \sqrt{\alpha\alpha'} \epsilon \cos^2 \theta_\epsilon}{2q^2 \cos\theta_W (1 - \epsilon^2)} \right)^2 \text{tr}[(\gamma^\mu p'_\mu - \mathbf{1} m_f) \gamma^\nu (\gamma^\rho p_\rho + \mathbf{1} m_f) \gamma^\sigma] \text{tr}[(\gamma^\alpha k_{DM\alpha} + \mathbf{1} m_{DM}) \gamma^\beta (\gamma^\delta k'_{DM\delta} - \mathbf{1} m_{DM}) \gamma^\epsilon] \quad (\text{A.6})$$

For the t channel scattering process of SM particles and DM particles, we have a very similar expression with a few minor changes.

If the fermion anti-fermion momenta were p, p' and k, k' respectively, they can now be written as $p \rightarrow p_1, p' \rightarrow -p'_1$. Similarly, the DM momenta terms change as, $k \rightarrow p'_2$ and $k' \rightarrow -p_2$. This is related to the fact that we rotate the Feynman diagram, and in the new diagram, the directions of \bar{p} and \bar{k}_{DM} are simply reversed. Therefore we have (Using the slash notation now instead of the $\gamma^\mu p_\mu$ summation notation),

$$\left(\frac{K_i 4\pi \sqrt{\alpha\alpha'} \epsilon \cos^2 \theta_\epsilon}{2q^2 \cos\theta_W (1 - \epsilon^2)} \right)^2 \text{tr}[(p'_1 + \mathbf{1} m_f) \gamma^\mu (p_1 + \mathbf{1} m_f) \gamma^\nu] \text{tr}[(p'_2 + \mathbf{1} m_{DM}) \gamma_\mu (p_2 + \mathbf{1} m_{DM}) \gamma_\nu] \quad (\text{A.7})$$

Given below is the Feynman Diagram of the first kind in [2.7](#), the calculation for which, and the corresponding t-channel diagram is shown above.



We can simplify both the s-channel and t channel diagrams by using the Clifford algebra properties of the gamma matrices and the consequent properties of their traces. A summary of the trace properties would be as follows,

$$* \text{tr}(\mathbf{1}) = 4$$

$$* \text{tr}(\gamma^\mu) = 0$$

*tr(odd number of gamma matrices multiplied to each other) = 0 (use $\text{tr}(\gamma^5\gamma^5) = 1$ to show $\text{tr}(x) = -\text{tr}(x)$)

$$* \text{tr}(\gamma^\mu\gamma^\nu) = 4g^{\mu\nu} \text{ (use the property, } \gamma^\mu\gamma^\nu = 2g^{\mu\nu}\mathbb{1}\text{)}$$

$$*\text{tr}(\gamma^5) = 0$$

$$*\text{tr}(\gamma^\mu\gamma^\nu\gamma^\rho\gamma^\sigma\gamma^5) = -4i\epsilon^{\mu\nu\rho\sigma}$$

$$*\text{tr}(\gamma^\mu\gamma^\nu\gamma^\rho\gamma^\sigma) = 4(g^{\mu\nu}g^{\rho\sigma} - g^{\mu\rho}g^{\nu\sigma} + g^{\mu\sigma}g^{\nu\rho})$$

Upon using the above properties we can simplify equation 22 for the s-channel as,

$$8 \left(\frac{K_i 4\pi \sqrt{\alpha\alpha'} \epsilon \cos^2 \theta_\epsilon}{q^2 \cos \theta_W (1 - \epsilon^2)} \right)^2 [(p \cdot k)(p' \cdot k') + (p \cdot k')(p' \cdot k) + m_f^2(k \cdot k') + m_{DM}^2(p \cdot p') + 2m_f^2 m_{DM}^2] \quad (\text{A.8})$$

We can make our life lot simpler by representing all the p_i 's in terms of the energies and subsequently in terms of the Mandelstam variable s and other constants/parameters like the various masses and couplings. Note that it is easier to integrate over s since it varies from $2m_f^2$ to infinity. But the functional form inside the integral is converging, and thus we can terminate our limit to a high enough value to get an approximate result, computationally.

If initial energies of the particle is given by E_1 and E_2 , in CM frame for particle anti-particle annihilation, using energy conservation, we can use the following,

$$q^2 = (p + p')^2 = 4E^2 = s$$

$$p \cdot p' = E^2 + |p|^2 = s/2$$

$$k \cdot k' = E^2 + |k|^2 = s/2$$

$$p \cdot k = p' \cdot k' = E^2 - |p||k|\cos\theta = -(t - m_{DM}^2 - m_f^2)/2$$

$$p \cdot k' = p' \cdot k = E^2 + |p||k|\cos\theta = -(u - m_{DM}^2 - m_f^2)/2$$

$$|k|^2 = E^2 - m_{DM}^2$$

$$|p|^2 = E^2 - m_f^2$$

(using)

$$t = (k - p)^2 = (k' - p')^2$$

$$t = (k - p')^2 = (k' - p)^2$$

$$p^2 = p'^2 = m_f^2$$

$$k^2 = k'^2 = m_{DM}^2$$

to write the RHS further as,

$$8 \left(\frac{K_i 4\pi \sqrt{\alpha\alpha'} \epsilon \cos^2 \theta_\epsilon}{4E^2 \cos \theta_W} \right)^2 [(E - |p||k| \cos \theta)^2 + (E + |p||k| \cos \theta)^2 + m_{DM}^2(E^2 + |p|^2)]$$

$$[+m_f^2(E^2 + |k|^2) + 2m_{DM}^2 m_f^2]$$

$$(8/16) \left(\frac{K_i 4\pi \sqrt{\alpha\alpha'} \epsilon \cos^2 \theta_\epsilon}{\cos \theta_W} \right)^2 \left[2 + \frac{2(E^2 - m_f^2)(E^2 - m_{DM}^2)}{E^4} + \frac{m_{DM}^2(2E^2 - m_f^2)}{E^4} \right]$$

$$\left[+\frac{m_f^2(2E^2 - m_{DM}^2)}{E^4} + \frac{2m_{DM}^2 m_f^2}{E^4} \right]$$

Upon re-arranging we get,

$$\left(\frac{K_i 4\pi \sqrt{\alpha\alpha'} \epsilon \cos^2 \theta_\epsilon}{\cos \theta_W} \right)^2 \left[1 + \frac{m_{DM}^2 + m_f^2}{E^2} + \cos^2 \theta \left(1 - \frac{m_{DM}^2 + m_f^2}{E^2} + \frac{m_f^2 m_{DM}^2}{E^4} \right) \right]$$

Going from $|M|^2$ to σ we make the following adjustments

$$\frac{d\sigma}{d\Omega} = \frac{|k|}{2E_{CM}^2 16\pi^2 E_{CM}} \left(\frac{K_i 4\pi \sqrt{\alpha\alpha'} \epsilon \cos^2 \theta_\epsilon}{\cos \theta_W} \right)^2 |M'|^2 \quad (\text{A.9})$$

Finally giving us,

$$\frac{d\sigma}{d\Omega} = \frac{K_i^2 \kappa^2 \alpha^2 \cos^4 \theta_\epsilon}{4E_{CM}^2 \cos^2 \theta_W} \sqrt{1 - \frac{m_{DM}^2}{E^2}} \left[1 + \frac{m_{DM}^2 + m_f^2}{E^2} + \cos^2 \theta \left(1 - \frac{m_{DM}^2 + m_f^2}{E^2} + \frac{m_f^2 m_{DM}^2}{E^4} \right) \right] \quad (\text{A.10})$$

After integrating across θ from 0 to π , we can get to the final expression,

$$\frac{d\sigma}{d\Omega} = \frac{\pi K_i^2 \kappa^2 \alpha^2 \cos^4 \theta_\epsilon}{E_{CM}^2 \cos^2 \theta_W} \sqrt{1 - \frac{m_{DM}^2}{E^2}} \left[1 + \frac{m_f^2 + m_{DM}^2}{E^2} + \frac{E^2 - m_f^2 + m_{DM}^2 + 4m_f^2 m_{DM}^2}{E^2} \right] \quad (\text{A.11})$$

putting $E^2 = E_{cm}^2/4 = s/4$ we get,

$$\frac{d\sigma}{d\Omega} = \frac{\pi K_i^2 \kappa^2 \alpha^2 \cos^4 \theta_\epsilon}{s \cos^2 \theta_W} \sqrt{1 - \frac{m_{DM}^2}{E^2}} \left[1 + \frac{4m_f^2 + 4m_{DM}^2}{s} + \frac{s - 4m_f^2 + 4m_{DM}^2 + 16m_f^2 m_{DM}^2}{3s} \right] \quad (\text{A.12})$$

If we are to write everything in equation [A.12](#) in terms of the Mandelstam variables and particle masses as shown, we have an expression,

$$8 \left(\frac{K_i 4\pi \sqrt{\alpha\alpha'} \epsilon \cos^2 \theta_\epsilon}{q^2 \cos \theta_W (1 - \epsilon^2)} \right)^2 \left[\frac{(t - m_{DM}^2 - m_f^2)^2}{4} + \frac{(u - m_{DM}^2 - m_f^2)^2}{4} + \frac{s(m_f^2 + m_{DM}^2)}{2} \right]$$

And similarly, we can simplify equation 23 for the t-channel as,

$$8 \left(\frac{K_i 4\pi \sqrt{\alpha\alpha'} \epsilon \cos^2 \theta_\epsilon}{q^2 \cos \theta_W (1 - \epsilon^2)} \right)^2 [(p_1 \cdot p'_2)(p'_1 \cdot p_2) + (p_1 \cdot p_2)(p'_1 \cdot p'_2) - m_f^2(p_2 \cdot p'_2) - m_{DM}^2(p_1 \cdot p'_1) + 4m_f^2 m_{DM}^2] \quad (\text{A.13})$$

For the fourth type of Feynman diagram that we see in [2.7](#) shall be considering, to be used in the Boltzman code, we shall be using the fermion propagator and external photon lines (for both directions with respect to the time direction), which were not used before. This is diagram comprises of only the dark sector fermions and bosons. In Compton scattering, as presented below, all the momenta directions are along the time direction, which makes writing the cross section matrix simpler, after which we simply employ crossing symmetry to reach the required Feynman diagram by making the necessary changes in the momenta directions. Using the standard Feynman rules where we go along one direction (either along the time direction, or against) we see that, for the Compton scattering case $|iM|$ can be written as,

$$iM = \bar{u}(p')(-ie\gamma^\mu)\epsilon_\mu^*(k') \frac{i(p+k+m_{DM})}{(p+k)^2 - m_{DM}^2} (-ie\gamma^\nu)\epsilon_\nu(k)u(p) \\ + \bar{u}(p')(-ie\gamma^\nu)\epsilon_\nu(k) \frac{i(p-k'+m_{DM})}{(p-k')^2 - m_{DM}^2} (-ie\gamma^\mu)\epsilon_\mu^*(k')u(p)$$

Here, the two terms summed together are due to the fact that, we can have two cases of Compton scattering with the directions of the respective momenta of the vector boson interacting with the particle interchanged. It is similar to a difference between a t channel and u channel diagram if I am to draw a rough analogy. Compton scattering diagrams depicted below. ϵ and ϵ^* depict the polarization vector associated to the two photons with

their respective momenta(k and k') as shown.

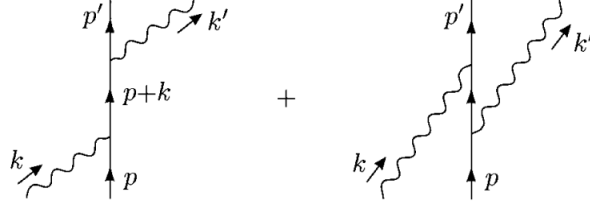


Figure A.1: In the two-photon production case, our momenta associated to the external lines as in the above case change as, $p \rightarrow p_1$, $p' \rightarrow -p_2$, $k \rightarrow -k_1$, $k' \rightarrow -k_2$, as will be calculated. This change owes to the crossing symmetry between the Compton scattering process and the release of two photons process.

Upon some simplifications i.e., using the standard, $p^2 = m^2$ and $k^2 = 0$ we can use, $(p + k)^2 - m^2 = 2p \cdot k$ and $(p - k')^2 - m^2 = -2p \cdot k'$.

And for the later part in both the terms summed together, we can use the result derived using some Clifford algebra,

$$\begin{aligned} (p + m)\gamma^\nu u(p) &= (2p^\nu - \gamma^\nu p + \gamma^\nu m)u(p) \\ &= 2p^\nu u(p) - \gamma^\nu (p - m)u(p) \end{aligned}$$

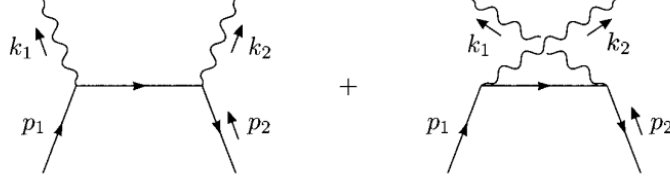
and, using the dirac equation, we can set the second term to 0, therefore getting

$$(p + m)\gamma^\nu u(p) = 2p^\nu u(p) \tag{A.14}$$

$$iM = ie^2 \epsilon_\mu^*(k') \epsilon_\nu(k) \bar{u}(p') \left[\frac{\gamma^\mu k \gamma^\nu + 2\gamma^\mu p^\nu}{2p \cdot k} + \frac{-\gamma^\nu k' \gamma^\mu + 2\gamma^\nu p^\mu}{-2p \cdot k'} \right] u(p) \tag{A.15}$$

Using further trace calculations and manipulations as described in the s-channel and t-channel cases, for which I shall provide a reference and detailed calculations to, we get to the final expression,

$$\frac{1}{4} \sum_{spins} |M|^2 = 2e^4 \left[\frac{p \cdot k'}{p \cdot k} + \frac{p \cdot k}{p \cdot k'} + 2m^2 \left(\frac{1}{p \cdot k} - \frac{1}{p \cdot k'} \right) + m^4 \left(\frac{1}{p \cdot k} - \frac{1}{p \cdot k'} \right)^2 \right] \quad (\text{A.16})$$



This process is related to Compton scattering by crossing symmetry; we can obtain the correct amplitude from the Compton amplitude by making the replacements

$$p \rightarrow p_1 \quad p' \rightarrow -p_2 \quad k \rightarrow -k_1 \quad k' \rightarrow k_2.$$

Figure A.2: Diagram for two hidden sector fermions giving rise to two dark photons. The internal particle propagator must have a three momentum given by $p_1 - k_1$, due to conservation of momentum. Ref: M. Peskin, E. Shroeder Introduction to QFT

Now, looking at the 2 photon (dark) annihilation process, we must make the necessary changes in momenta notations, signs, which can be derived using the crossing symmetry, and coupling constants as shown above. The desired expression looks like,

$$\frac{1}{4} \sum_{spins} |M|^2 = -2(4\pi\alpha')^2 \left[\frac{p_1 \cdot k_2}{p_1 \cdot k_1} + \frac{p_1 \cdot k_1}{p_1 \cdot k_2} + 2m^2 \left(\frac{1}{p_1 \cdot k_1} - \frac{1}{p_1 \cdot k_2} \right) - m^4 \left(\frac{1}{p_1 \cdot k_1} + \frac{1}{p_1 \cdot k_2} \right)^2 \right] \quad (\text{A.17})$$

Note that as before, this equation represents a superposition of two kinds of double (dark) photon annihilation, with the directions of the vector bosons interchanged.

In terms of initial energy of the dark fermion in the CM frame, the expression for $\frac{d\sigma}{d\cos\theta}$ which contains the above, $\frac{1}{4} \sum_{spins} |M|^2$ term, in the high energy limit is,

$$\frac{d\sigma}{d\cos\theta} = \frac{2\pi\alpha'^2}{s} \left(\frac{1 + \cos^2\theta}{\sin^2\theta} \right) \quad (\text{A.18})$$

Here s , the Mandetstam variable is equal to the total energy of the incoming particle in

the CM frame.

However for our case, we cannot be using the High Energy Approximation just yet, as we must keep room for large DM masses too. As a result, we simply try an simplify the expression [A.17](#) in terms of s .

We intend to write the expression in terms of the laboratory friendly quantities, s and θ s. The detailed calculations are shown in the appendix* .

Thhe Final expression which we have for $\sigma(s)$ for the two photon release channel, looks like,

$$\sigma = \frac{\pi\kappa^4\alpha^2}{2\epsilon^4s} \sqrt{\frac{s}{s-4m^2}} \left[\frac{16m^4}{s(s/4-m^2)-s^2/4} - 4 - \ln \left| \frac{(s/4-m^2) - \sqrt{s/4(s/4-m^2)}}{(s/4-m^2) + \sqrt{s/4(s/4-m^2)}} \right| \cdot A \right] \quad (\text{A.19})$$

where A is,

$$\frac{s(s+4m^2)-8m^4}{s\sqrt{s/4(s/4-m^2)}} \quad (\text{A.20})$$

Calling the RHS of equation 27 as I, equation 28 as II and equation 34 as III, we finally substitute them in $\sigma(s)$ of the following Boltzmann equation which was mentioned before, to get a final result for the most general form.

$$\frac{d(\frac{\rho'}{\rho})}{dT} = -\frac{g_1g_2}{H(T)T\rho^32\pi^4} \int ds \cdot \sigma(s)(s-4m^2)sTK_2\left(\frac{\sqrt{s}}{T}\right)$$

Recall, $\sigma(s)$ had the form,

$$\sigma(s) \equiv \frac{1}{2E_12E_2v_{mol}} \int \prod_{i=3}^4 d^3\vec{p}_i \cdot g_i |\iota M|^2 (2\pi)^4 \delta^{(4)}(\Sigma p_i^{s,t,u}) \quad (\text{A.21})$$

A.1.1 Z-Resonances

In theory we must also involve the Z-Boson which we ignored in our calculations before. It introduces the phenomena of Z- resonances which must give rise to some unique structures in our plots. The conservation laws are exactly the same as in QED+ (i.e. QED with the presence of the Z Boson). Conservation of lepton number. Therefore analogously, we might consider conserving the dark fermions too, in our diagram. We also have the usual conservation laws: energy, momentum, angular momentum. The Z boson is heavy, roughly 91 GeV. Thus we might want to look at it as some massive version of the photon with similar properties but the corresponding coupling constants. The Z boson is usually virtual. It only exists quantum mechanically and is never directly measured(quickly decays in general due to it's unstable, high mass). Since it is virtual this process occurs even when the participating fermions (leptons) are not energetic enough to produce a physical Z boson. But when the electrons have just enough energy to produce a physical Z; the process goes “on shell” and is greatly enhanced. This is the phenomena of Z-resonance.

The final expression for the total cross section element for the Z boson pathway looks like,

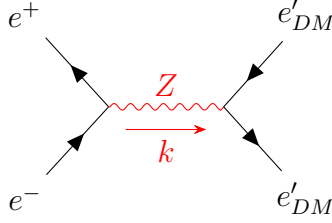
$$\sigma_{e^+e^-ZDMDM} = \frac{sg^2g_{DM}^2}{192\pi((s - m_Z^2)^2 + (m_Z\Gamma_Z)^2)} [(c_V^e)^2 + (c_A^e)^2][(c_V^{DM})^2 + (c_A^{DM})^2] \quad (\text{A.22})$$

$$\sigma_{e^+e^-ZDMDM} = \frac{sg^2g_{DM}^2}{192\pi((s - m_Z^2)^2 + (m_Z\Gamma_Z)^2)} K \quad (\text{A.23})$$

with g being the usual coupling constant for the weak interaction and g_{DM} being,

$$g_{DM} = -\frac{e'\epsilon\sin\theta_\epsilon}{\sqrt{1-\epsilon^2}} = -\frac{\sqrt{4\pi\alpha'}\epsilon\sin\theta_\epsilon}{\sqrt{1-\epsilon^2}} \quad (\text{A.24})$$

A detailed calculation for the same is as below (starting with the simple case of a decay mode into electrons and positrons only)-



We have the $e^+ e^-$ vertex which can be given as,

$$\bar{v}(p_2) \cdot (-ig_Z \gamma^\mu) \frac{1}{2} (c_V^e - c_A^e \gamma^5) u(p_1)$$

with subscripts v and A denoting the vertical and axial components of the vertex coupling respectively.

The Z propagator is given by, $(-ig_{\mu\nu}/q^2 - m_Z^2)$

The $e_{DM} e'_{DM}$ vertex term looks like,

$$\bar{u}_{DM}(p_3) \cdot (-ig'_Z \gamma^\nu) \frac{1}{2} (c_V^{DM} - c_A^{DM} \gamma^5) v_{DM}(p_4)$$

Leaving us with a scattering amplitude of the form,

$$M = \left(\frac{-g_Z g'_Z}{q^2 - m_Z^2} \right) g_{\mu\nu} \left[\bar{v}(p_2) \gamma^\mu \frac{1}{2} (c_V^e - c_A^e \gamma^5) u(p_1) \right] \left[\bar{u}_{DM}(p_3) (\gamma^\nu) \frac{1}{2} (c_V^{DM} - c_A^{DM} \gamma^5) v_{DM}(p_4) \right]$$

Here, $g_Z = -g \cos \theta_W / \cos \theta_\epsilon$; $g'_Z = -e' \epsilon \sin \theta_\epsilon / \sqrt{1 - \epsilon^2}$ Also, let $c_V = c_L + c_R$, $c_A = (c_L - c_R)$

Therefore we can write,

$$\begin{aligned} \frac{1}{2} (c_V - c_A \gamma^5) &= \frac{1}{2} (c_L + c_R - (c_L - c_R) \gamma^5) \\ &= \frac{1}{2} c_L (1 - \gamma^5) + \frac{1}{2} c_R (1 + \gamma^5) \end{aligned}$$

also, we shall use, $(1 - \gamma^5)u = 2u_L$, $(1 + \gamma^5)u = 2u_R$ and so on.

We can therefore re-write the resulting scattering amplitude as,

$$M_{fi} = \left(\frac{-g_Z g_{Z'}}{q^2 - m_Z^2} \right) g_{\mu\nu} [c_L^e \bar{v}(p_2) \gamma^\mu u_L(p_1) + c_R^e \bar{v} \gamma^\mu u_R(p_2)] \\ \cdot [c_L^{DM} \bar{u}_{DM}(p_3) \gamma^\nu v_{DMR}(p_4) + c_R^{DM} \bar{u}_{DM}(p_3) \gamma^\nu v_{DML}(p_4)]$$

using, $\bar{u}_R \gamma^\mu v_R$, $\bar{u}_L \gamma^\mu v_L = 0$ and similarly for the DM terms, we can write,

$$M_{fi} = \left(\frac{-g_Z g_{Z'}}{q^2 - m_Z^2} \right) g_{\mu\nu} [c_L^e \bar{v}_R(p_2) \gamma^\mu u_L(p_1) + c_R^e \bar{v}_L \gamma^\mu u_R(p_2)] \\ \cdot [c_L^{DM} \bar{u}_{DML}(p_3) \gamma^\nu v_{DMR}(p_4) + c_R^{DM} \bar{u}_{DMR}(p_3) \gamma^\nu v_{DML}(p_4)]$$

Quite clearly, upon expanding the scattering amplitude which we have now written in terms of the left handed and right handed components of the particle fields, we shall now have terms in the scattering amplitude M, proportional to,

$$M_{RR} \propto [\bar{v}_L(p_2) \gamma^\mu u_R(p_1)] [\bar{u}_{DMR}(p_3) \gamma^\nu v_{DML}(p_4)] = s(1 + \cos\theta)$$

$$M_{RL} \propto [\bar{v}_L(p_2) \gamma^\mu u_R(p_1)] [\bar{u}_{DML}(p_3) \gamma^\nu v_{DMR}(p_4)] = s(1 - \cos\theta)$$

$$M_{LL} \propto [\bar{v}_R(p_2) \gamma^\mu u_L(p_1)] [\bar{u}_{DMR}(p_3) \gamma^\nu v_{DML}(p_4)] = s(1 - \cos\theta)$$

$$M_{RL} \propto [\bar{v}_R(p_2) \gamma^\mu u_L(p_1)] [\bar{u}_{DML}(p_3) \gamma^\nu v_{DMR}(p_4)] = s(1 + \cos\theta)$$

with $q^2 = s = E_{CM}^2$. Therefore, we finally get terms like

$$\begin{aligned}
|M_{RR}|^2 &= s^2 \left| \frac{-g_Z g_{Z'}}{q^2 - m_Z^2} \right| (c_R^e c^{DM_R})^2 (1 + \cos^2 \theta) \\
|M_{RL}|^2 &= s^2 \left| \frac{-g_Z g_{Z'}}{q^2 - m_Z^2} \right| (c_R^e c^{DM_L})^2 (1 - \cos^2 \theta) \\
|M_{LR}|^2 &= s^2 \left| \frac{-g_Z g_{Z'}}{q^2 - m_Z^2} \right| (c_L^e c^{DM_R})^2 (1 - \cos^2 \theta) \\
|M_{LL}|^2 &= s^2 \left| \frac{-g_Z g_{Z'}}{q^2 - m_Z^2} \right| (c_L^e c^{DM_L})^2 (1 + \cos^2 \theta)
\end{aligned}$$

which are a lot more neat and can be used in the final expression.

We also need to keep in mind that while dealing with a massive mediator, the mass term in the denominator of the propagator can create a divergence while we integrate the scattering amplitudes. In-order to prevent this we use a Breit Wigner Resonance distribution, instead of allowing the mass term to cancel s at $s = \sqrt{m_Z}$. Also, the Z boson is a heavy and an unstable particle which tends to decay into other lighter particles associated with a corresponding lifetime for the decay.

For a stable particle we roughly use,

$$\psi \approx e^{-imt}$$

where, ψ denotes the approximate wave-function for the sub-atomic particle. For a heavy and an unstable Z -boson, we modify the above as,

$$\psi \approx e^{-imt} e^{-\Gamma_Z t/2}$$

with $\tau = 1/\Gamma_Z$. Applying the Breit-Wigner modification, we shall change the mass term in our earlier expression as,

$$m \rightarrow m - \frac{i\Gamma_Z}{2}$$

Thereby modifying,

$$\left| \frac{1}{s - m_Z^2} \right|^2 \rightarrow \left| \frac{1}{s - m_Z^2 + im_Z \Gamma_Z} \right|^2$$

Finally, using (as shown before)

$$\frac{d\sigma}{d\Omega} = \frac{|M_{fi}|^2}{64s\pi^2}$$

and

$$|M_{fi}|^2 = \frac{1}{4} (|M_{RR}|^2 + |M_{RL}|^2 + |M_{LR}|^2 + |M_{LL}|^2)$$

We get,

$$\frac{d\sigma}{d\Omega} = \frac{(g_Z g'_Z)^2}{64s\pi^2((s - m_Z^2)^2 - m_Z^2 \Gamma_Z^2)} \left(\frac{1}{4} [(c_V^e)^2 + (c_A^e)^2] [(c_V^{DM})^2 + (c_A^{DM})^2] (1 + \cos^2\theta) + 2c_V^e c_A^e c_V^{DM} c_A^{DM} \cos\theta \right) \quad (\text{A.25})$$

Integrating over the solid angle and therefore using,

$$\int_{-1}^1 (1 + \cos^2\theta) d\cos\theta = \frac{8}{3}$$

$$\int_{-1}^1 (\cos\theta) d\cos\theta = 0$$

We finally have,

$$\sigma = \frac{(g_Z g'_Z)^2}{192\pi s((s - m_Z^2)^2 - m_Z^2 \Gamma_Z^2)} ([(c_V^e)^2 + (c_A^e)^2] [(c_V^{DM})^2 + (c_A^{DM})^2]) \quad (\text{A.26})$$

We put all of the scattering cross-sections in [2.21](#) or [2.28](#) as used in the Boltzmann solver and run the code to have an idea of the expected RDs. As we learnt, varying the parameters plays a crucial role in. Thereby, we have explored the theoretical base of all the fancy codes written and all the seemingly simple calculations performed, by advanced DM codes, and gather a better understanding of what goes on underneath the glamour.

A.2 Calculation of σ for the release of dark photons from dark fermions in terms of s

We start from (with the crossing symmetry applied to the Compton scattering process) [A.17](#),

$$\frac{1}{4} \sum_{spins} |M|^2 = -2(4\pi\alpha')^2 \left[\frac{p_1 \cdot k_2}{p_1 \cdot k_1} + \frac{p_1 \cdot k_1}{p_1 \cdot k_2} + 2m^2 \left(\frac{1}{p_1 \cdot k_1} - \frac{1}{p_1 \cdot k_2} \right) - m^4 \left(\frac{1}{p_1 \cdot k_1} + \frac{1}{p_1 \cdot k_2} \right)^2 \right]$$

Moving from the scattering amplitude to the differential scattering cross-section element $d\sigma/d\cos\theta$, we can immediately make the following modification,

$$\frac{d\sigma}{d\cos\theta} = \frac{2\pi\alpha'^2}{s} \frac{E_{ini}}{|\vec{p}_{ini}|} \left[\frac{p_1 \cdot k_2}{p_1 \cdot k_1} + \frac{p_1 \cdot k_1}{p_1 \cdot k_2} + 2m^2 \left(\frac{1}{p_1 \cdot k_1} - \frac{1}{p_1 \cdot k_2} \right) - m^4 \left(\frac{1}{p_1 \cdot k_1} + \frac{1}{p_1 \cdot k_2} \right)^2 \right] \quad (\text{A.27})$$

which can be further written in terms of E and p as,

$$\frac{d\sigma}{d\cos\theta} = \frac{2\pi\alpha'^2}{s} \frac{E_{ini}}{|\vec{p}_{ini}|} \left[\frac{E^2 + (pcos\theta)^2}{m^2 + (psin\theta)^2} + \frac{2m^2}{m^2 + (psin\theta)^2} - \frac{2m^4}{(m^2 + (psin\theta)^2)^2} \right] \quad (\text{A.28})$$

Using the following labels and expressions from,

with,

$$\begin{aligned} s &= (p_1 + p_2)^2 = p_1^2 + p_2^2 + 2p_1 p_2 \\ &= E^2 - p^2 + E^2 - p^2 + 2(E^2 + p^2) = 4E^2 \\ p^2 &= E^2 - m^2 = \frac{s}{4} - m^2 \end{aligned}$$

Substituting the above we can then write the following version of [A.17](#),

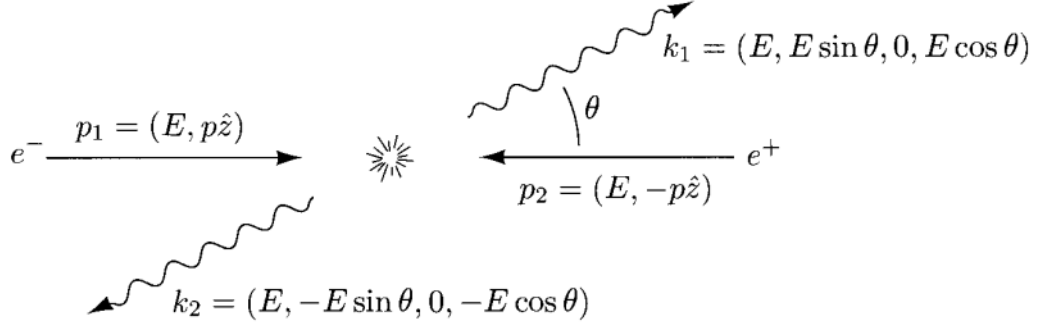


Figure A.3: Kinematics of the release of two dark photons process in the center of mass frame. Ref: M. Peskin, E. Shroeder Introduction to QFT

$$\begin{aligned} \frac{d\sigma}{d\cos\theta} &= \frac{2\pi\alpha'^2}{s} \frac{\sqrt{s}}{2\sqrt{s/4 - m^2}} \left[(1/4) \frac{(s + (s - 4m^2)\cos^2\theta) + 2m^2}{m^2 + (s/4 - m^2)\sin^2\theta} - \frac{2m^4}{(m^2 + (s/4 - m^2)\sin^2\theta)^2} \right] \\ &= \frac{\pi\alpha'}{2s} \sqrt{\frac{s}{s - 4m^2}} \left[\frac{(s - 4m^2)\cos^2\theta}{m^2 + (s/4 - m^2)\sin^2\theta} + \frac{s + 8m^2}{m^2 + (s/4 - m^2)\sin^2\theta} - \frac{8m^4}{(m^2 + (s/4 - m^2)\sin^2\theta)^2} \right] \end{aligned}$$

where the three terms inside the parenthesis are three different types of integral in terms of $\cos\theta$. Simplifying the expression (say writing the entire expression in terms of $\cos\theta$ only and calling it some variable x) and thereby performing three somewhat tedious but doable integrals, we reach the expression [A.19](#).

$$\sigma = \frac{\pi\kappa^4\alpha'^2}{2\epsilon^4 s} \sqrt{\frac{s}{s - 4m^2}} \left[\frac{16m^4}{s(s/4 - m^2) - s^2/4} - 4 - \ln \left| \frac{(s/4 - m^2) - \sqrt{s/4(s/4 - m^2)}}{(s/4 - m^2) + \sqrt{s/4(s/4 - m^2)}} \right| \cdot A \right]$$

A.3 Useful Dirac algebra properties and proofs

Proving,

$$\text{tr}(\gamma^\mu \gamma^\nu \gamma^\rho \gamma^\sigma) = 4(g^{\mu\nu} g^{\rho\sigma} - g^{\mu\rho} g^{\nu\sigma} + g^{\mu\sigma} g^{\nu\rho}) \quad (\text{A.29})$$

Using,

$$\gamma^\mu \gamma^\nu = 2g^{\mu\nu} \cdot \mathbb{1} - \gamma^\nu \gamma^\mu$$

which we derive from the anti-commutator property of two dirac matrices, γ^μ and γ^ν

We have (using the cyclicity of traces),

$$\begin{aligned} tr(\gamma^\mu \gamma^\nu) &= tr(2g^{\mu\nu} \cdot \mathbb{1} - \gamma^\nu \gamma^\mu) \\ &= 8g^{\mu\nu} - tr(\gamma^\mu \gamma^\nu) \\ &= 4g^{\mu\nu} \end{aligned}$$

$tr(\gamma^\mu \gamma^\nu \gamma^\rho \gamma^\sigma)$ can be written as,

$$tr(2g^{\mu\nu} \gamma^\rho \gamma^\sigma - \gamma^\nu \gamma^\mu \gamma^\rho \gamma^\sigma)$$

Adding and subtracting $\gamma^\nu 2g^{\mu\rho} \gamma^\sigma$ inside the trace on the RHS, and writing one of those terms as $\gamma^\nu \gamma^\rho 2g^{\mu\sigma}$ using the anti-commutator property of Gamma matrices we see,

$$\begin{aligned} tr(\gamma^\mu \gamma^\nu \gamma^\rho \gamma^\sigma) &= tr(2g^{\mu\nu} \gamma^\rho \gamma^\sigma - \gamma^\nu 2g^{\mu\rho} \gamma^\sigma + \gamma^\nu \gamma^\rho 2g^{\mu\sigma} - \gamma^\nu \gamma^\rho \gamma^\sigma \gamma^\mu) \\ &= (1/2)2 [g^{\mu\nu} tr \gamma^\rho \gamma^\sigma - g^{\mu\rho} tr \gamma^\nu \gamma^\sigma + g^{\mu\sigma} tr \gamma^\nu \gamma^\rho] \\ &= 4(g^{\mu\nu} g^{\rho\sigma} - g^{\mu\rho} g^{\nu\sigma} + g^{\mu\sigma} g^{\nu\rho}) \end{aligned}$$

where we used $tr(\gamma^\mu \gamma^\nu) = 4g^{\mu\nu}$ as shown, to get to the last step.

We now return to the evaluation of the squared matrix element in [A.7](#). We expand,

$$tr [(p' - m_f) \gamma^\nu (p + m_f) \gamma^\rho] = tr [(p' p) \gamma^\mu \gamma^\nu \gamma^\rho \gamma^\sigma - m_f^2 \gamma^\nu \gamma^\sigma - m_f p \gamma^\nu \gamma^\rho \gamma^\sigma + p' m_f \gamma^\mu \gamma^\nu \gamma^\sigma]$$

(where we have used the fact that the trace of an odd number of matrices is zero to

cancel the last two terms)

Using the earlier results obtained for traces of the product of even number of matrices we get to,

$$4 [p'^{\mu} p^{\nu} + p'^{\nu} p^{\mu} - g^{\mu\nu} (p \cdot p' + m_f^2)]$$

Similarly, for the second part we have,

$$tr [(k^{DM} + m_{DM})\gamma^{\beta}(k'_{DM} - m_{DM})\gamma^{\epsilon}] = 4 [k_{\mu}k'_{\nu} + k_{\nu}k'_{\mu} - g_{\mu\nu}(k_{DM} \cdot k'_{DM} + m_{DM}^2)]$$

Finally we substitute the results into the relevant expressions to get the following expression which upon some modification gives us [A.8](#),

$$8[(p \cdot k)(p' \cdot k') + (p \cdot k')(p' \cdot k) + m_f^2(k \cdot k') + m_{DM}^2(p \cdot p') + 4m_f^2 m_{DM}^2]$$

Bibliography

- [1] A Arbey and F Mahmoudi. Dark matter and the early universe: A review. *Progress in Particle and Nuclear Physics*, page 103865, 2021.
- [2] Gianfranco Bertone, Dan Hooper, and Joseph Silk. Particle dark matter: Evidence, candidates and constraints. *Physics reports*, 405(5-6):279–390, 2005.
- [3] Mariangela Lisanti. Lectures on dark matter physics. In *New Frontiers in Fields and Strings: TASI 2015 Proceedings of the 2015 Theoretical Advanced Study Institute in Elementary Particle Physics*, pages 399–446. World Scientific, 2017.
- [4] Xiaoyong Chu, Thomas Hambye, and Michel HG Tytgat. The four basic ways of creating dark matter through a portal. *Journal of Cosmology and Astroparticle Physics*, 2012(05):034, 2012.
- [5] Chiara Arina, Jan Heisig, Fabio Maltoni, Luca Mantani, Daniele Massaro, Olivier Matelaer, and Gopolang Mohlabeng. Studying dark matter with maddm 3.1: a short user guide. *arXiv preprint arXiv:2012.09016*, 2020.
- [6] Giorgio Arcadi, Abdelhak Djouadi, and Martti Raidal. Dark matter through the higgs portal. *Physics Reports*, 842:1–180, 2020.
- [7] Paolo Gondolo and Graciela Gelmini. Cosmic abundances of stable particles: improved analysis. *Nuclear Physics B - NUCL PHYS B*, 360:145–179, 08 1991.
- [8] Hugues Beauchesne, Enrico Bertuzzo, and Giovanni Grilli di Cortona. Dark matter in hidden valley models with stable and unstable light dark mesons. *Journal of High Energy Physics*, 2019(4):1–24, 2019.
- [9] Subhaditya Bhattacharya, Blaženka Melić, and Jose Wudka. Pionic dark matter. *Journal of High Energy Physics*, 2014(2):1–38, 2014.
- [10] Hugues Beauchesne and Giovanni Grilli di Cortona. Classification of dark pion multiplets as dark matter candidates and collider phenomenology. *Journal of High Energy Physics*, 2020(2):1–42, 2020.

- [11] Hsin-Chia Cheng, Lingfeng Li, and Ennio Salvioni. A theory of dark pions. *Journal of High Energy Physics*, 2022(1):1–52, 2022.
- [12] Thomas Hambye and Laurent Vanderheyden. Minimal self-interacting dark matter models with light mediator. *Journal of Cosmology and Astroparticle Physics*, 2020(05):001, 2020.
- [13] G Belanger, F Boudjema, and A Pukhov. micromegas: a code for the calculation of dark matter properties in generic models of particle interaction. *arXiv preprint arXiv:1402.0787*, 2014.
- [14] Alexander Pukhova. Pos (comptools2021) 037 an introduction to micromegas. 2021.
- [15] JA Casas, Manimala Chakraborti, and Javier Quilis. Uv completion of an axial, leptophobic, z . *Physics Letters B*, 809:135721, 2020.
- [16] Marco Cirelli, Gennaro Corcella, Andi Hektor, Gert Hütsi, Mario Kadastik, Paolo Panci, Martti Raidal, Filippo Sala, and Alessandro Strumia. Pppc 4 dm id: a poor particle physicist cookbook for dark matter indirect detection. *Journal of Cosmology and Astroparticle Physics*, 2011(03):051, 2011.
- [17] Christian Bierlich, Smitta Chakraborty, Nishita Desai, Leif Gellersen, Ilkka Helenius, Philip Ilten, Leif Lönnblad, Stephen Mrenna, Stefan Prestel, Christian Tobias Preuss, et al. A comprehensive guide to the physics and usage of pythia 8.3. *SciPost Physics Codebases*, page 008, 2022.
- [18] The Cherenkov Telescope Array Consortium, A Acharyya, R Adam, C Adams, I Agudo, A Aguirre-Santaella, R Alfaro, J Alfaro, C Alispach, R Aloisio, et al. Sensitivity of the cherenkov telescope array to a dark matter signal from the galactic centre. *arXiv preprint arXiv:2007.16129*, 2020.
- [19] HESS Collaboration, H Abdalla, F Aharonian, F Ait Benkhali, EO Anguner, C Armand, H Ashkar, M Backes, V Baghmanyany, V Barbosa Martins, et al. Search for dark matter annihilation signals in the hess inner galaxy survey. *arXiv preprint arXiv:2207.10471*, 2022.
- [20] Patrizia A Caraveo. The golden age of high-energy gamma-ray astronomy: the cherenkov telescope array in the multimessenger era. *La Rivista Del Nuovo Cimento*, 43(6):281–318, 2020.